Activity dependent Clustering of Neuronal L-Type Calcium Channels by CaMKII

Qian Yang[1], Lan Hu[1], Dorian Lawson-Qureshi[1], Roger J. Colbran[1,2,3]

[1]Department of Molecular Physiology and Biophysics
[2]Vanderbilt Brain Institute
[3]Vanderbilt-Kennedy Center for Research on Human Development,
Vanderbilt University School of Medicine, Nashville, TN, USA 37232-0615

Address correspondence to: Roger J. Colbran, Rm. 702 Light Hall, Vanderbilt University School of Medicine, Nashville, TN 37232-0615 (Tel: 615-936-1630. Fax: 615-322-7236. Email: roger.colbran@vanderbilt.edu)

ORCID IDs:
Qian Yang, 0000-0001-9861-2790
Roger J. Colbran, 0000-0001-7401-8244.

Abbreviations

APV	D-2-amino-5-phosphonovalerate
BayK	BayK-8644
CaMKII	Calcium/calmodulin-dependent protein kinase II
CaMKII-sh	shRNAs targeting CaMKIIα and CaMKIIβ
CNQX	6-Cyano-7-nitroquinoxaline-2,3-dione disodium
E-T coupling	excitation-transcription coupling
GFP	enhanced green fluorescent protein
GST	Glutathione-S-transferase
HA	Hemagglutinin
ICQ	intensity correlation quotient
iHA	intracellular HA-tag
LTCC	L-type calcium channel
Nssh	nonsense-shRNA
PDZ domain	PSD95/DlgA/Zo-1 domain
pCREB	Ser133 phosphorylation of CREB
ROI	region of interest
SAM	Sterile alpha motif
sHA	extracellular HA tag
TIRF	Total internal reflection fluorescence
TTX	tetrodotoxin
WT	wild type

Abstract

Neuronal excitation-transcription (E-T) coupling pathways can be initiated by local increases of Ca^{2+} concentrations within a nanodomain close to the L-type voltage-gated Ca^{2+} channel (LTCC). However, molecular mechanisms controlling LTCC organization within the plasma membrane that help creation these localized signaling domains remain poorly characterized. Here, we report that neuronal depolarization increases $Ca_V1.3$ LTCC clustering in cultured hippocampal neurons. Our previous work showed that binding of the activated catalytic domain of Ca^{2+}/calmodulin-dependent protein kinase II (CaMKII) to an RKR motif in the N-terminal cytoplasmic domain of $Ca_V1.3$ is required for LTCC-mediated E-T coupling. We tested whether multimeric CaMKIIα holoenzymes can bind simultaneously to co-expressed $Ca_V1.3$ α1 subunits with two different epitope tags. Co-immunoprecipitation assays from HEK293T cell lysates revealed that CaMKIIα assembles multimeric $Ca_V1.3$ LTCC complexes in a Ca^{2+}/calmodulin-dependent manner. CaMKII-dependent assembly of multi-$Ca_V1.3$ complexes is further facilitated by co-expression of the CaMKII-binding LTCC β2a subunit, relative to the β3 subunit, which cannot bind directly to CaMKII. Moreover, clustering of surface localized $Ca_V1.3$ α1 subunits in intact HEK293 cells was increased by pharmacological LTCC activation, but only in the presence of co-expressed wild-type CaMKIIα. Moreover, depolarization-induced clustering of surface-expressed $Ca_V1.3$ LTCCs in cultured hippocampal neurons was disrupted by suppressing the expression of CaMKIIα and CaMKIIβ using shRNAs. The CaMKII-binding RKR motif is conserved in the N-terminal domain of $Ca_V1.2$ α1 subunits and we found that activated CaMKIIα promoted the assembly of $Ca_V1.2$ homomeric complexes, as well as $Ca_V1.3$-$Ca_V1.2$ heteromeric complexes *in vitro*. Furthermore, neuronal depolarization enhanced the clustering of surface-expressed $Ca_V1.2$ LTCCs, and enhanced the colocalization of endogenous $Ca_V1.2$ LTCCs with surface-expressed $Ca_V1.3$, by CaMKII-dependent mechanisms. This work indicates that CaMKII activation-dependent LTCC clustering in the plasma membrane following neuronal depolarization may be essential for the initiation of a specific long-range signal to activate gene expression.

Introduction

Voltage-gated calcium channels are multi-subunit protein complexes consisting of a pore-forming α1 subunit and auxiliary β, α2, and δ subunits. The auxiliary subunits modulate the intrinsic biophysical and regulatory properties of the α1 subunit, and influence cell surface targeting (Richards *et al.* 2004; Voigt *et al.* 2016; Birnbaumer *et al.* 1998). The primary neuronal LTCC α1 subunits are $Ca_V1.2$ and $Ca_V1.3$, which exhibit highly overlapping expression patterns (Striessnig *et al.* 2014) and are often co-expressed in the same neuron. Although $Ca_V1.3$ is activated preferentially with more modest membrane depolarization (Koschak *et al.* 2001; Xu & Lipscombe 2001), $Ca_V1.2$ and $Ca_V1.3$ appear to regulate similar neuronal processes, such as excitation-transcription (E-T) coupling (Hetzenauer *et al.* 2006).

Learning and long-term memory require new gene transcription, which can be stimulated by many neurotransmitters. More specifically, LTCC-dependent E-T coupling links neuronal depolarization to the activation of several transcription factors that increase gene transcription (Ma *et al.* 2023), and can be initiated by locally elevated calcium concentrations near these

channels without requiring global calcium increases in the cytosol or nucleus (Wheeler *et al.* 2012). Single LTCCs can create local calcium nanodomains (Tadross *et al.* 2013; Nakamura *et al.* 2018) and it seems intuitive that the size and temporal dynamics of calcium nanodomains might be an important determinant of their biological function. However, the molecular mechanisms controlling LTCC calcium nanodomains are unclear. Previous studies revealed that LTCCs form clusters in the neuronal plasma membrane, and that clustering can facilitate the cooperative opening of some LTCC variants (Dixon *et al.* 2012; Moreno *et al.* 2016). Indeed, the cooperative opening of clustered LTCCs may substantially modify the characteristics of calcium nanodomains (Pfeiffer *et al.* 2020). Consequently, elucidating the molecular basis of LTCC clustering should provide new insights into the formation and function of calcium nanodomains.

LTCCs possess an intrinsic ability to form clusters (Moreno *et al.* 2016; Dixon *et al.* 2012). However, clustering may also be modulated by additional proteins that have been shown to interact with α1 or β auxiliary subunits to modulate LTCC intracellular trafficking and/or calcium influx (Weiss & Zamponi 2017), such as Shank3 or densin, postsynaptic scaffolding proteins (Zhang *et al.* 2005; Jenkins *et al.* 2010). Prior studies have also shown that calcium/calmodulin-dependent protein kinase II (CaMKII), a highly abundant postsynaptic protein kinase, can interact directly with multiple intracellular domains of the $Ca_V1.2$ or $Ca_V1.3$ α1 subunits (Hudmon *et al.* 2005; Wang *et al.* 2017; Simms *et al.* 2015), with β1 or β2a subunits (Grueter *et al.* 2008; Abiria & Colbran 2010), and also with densin (Strack *et al.* 2000; Jiao *et al.* 2011; Walikonis *et al.* 2001) and Shank3 (Perfitt *et al.* 2020; Cai *et al.* 2021) often facilitating calcium entry. Moreover, dodecameric CaMKII holoenzymes are capable of binding simultaneously to several other proteins, forming larger multi-protein complexes (Robison *et al.* 2005). Pharmacological and molecular studies have provided robust evidence that CaMKII is required for LTCC-dependent E-T coupling (Wheeler *et al.* 2008; Ma *et al.* 2014; Wang *et al.* 2017), at least in part by binding of activated CaMKII to RKR motifs in the N-terminal domain of $Ca_V1.3$ and in a central domain of Shank3 (Wheeler *et al.* 2008; Ma *et al.* 2014; Wang *et al.* 2017; Perfitt *et al.* 2020). Our recent work has shown that Shank3 can promote the clustering of neuronal $Ca_V1.3$ α1 subunits under basal conditions (Yang *et al.* 2023), but the specific role of CaMKII in LTCC clustering remains unknown.

Here, we show that CaMKII facilitates homo- or hetero-meric clustering of $Ca_V1.3$ or $Ca_V1.2$ complexes in an activation-dependent manner *in vitro* and on the membrane of HEK cells. This LTCC clustering requires direct interaction of CaMKII with $Ca_V1.3$ or $Ca_V1.2$ and is facilitated by β2a auxiliary subunits. Our data also indicate that neuronal depolarization promotes $Ca_V1.3$ and $Ca_V1.2$ LTCC membrane clustering in cultured hippocampal neurons, and that this clustering, as well as neuronal $Ca_V1.3$/$Ca_V1.2$ co-clustering, is disrupted by suppressing CaMKII expression. Collectively, our findings indicate that multimeric assembly of LTCCs following membrane depolarization, orchestrated by activated CaMKII, contributes to the initiation of E-T coupling mechanisms.

Method

DNA constructs

The original sources of all DNA constructs are provided in the Key Resources Table. All constructs were confirmed by DNA sequencing.

HEK cell culture and transfection

HEK293 and HEK293T cells (purchased from ATCC) were cultured and transfected as previously described (Yang *et al.* 2023). Briefly, cells were grown in high glucose DMEM at 37°C, 5% CO2, and passaged every 3-4 days. Cells (≤ 20 passages) were transfected using Lipofectamine 2000 after reaching approximately 70% confluence. Tagged $Ca_V1.3$ or/and $Ca_V1.2$ α1 subunits were always co-expressed with α2δ and either β3 or β2a with a FLAG tag (FLAG-β3 or -β2a) auxiliary subunits, together with pcDNA vector (empty or encoding CaMKIIα). The ratio of α1: α2δ: FLAG-β:pcDNA was set at 3:1:1:1.2. Co-transfections with N-terminal intracellular HA-tagged $Ca_V1.3$ (iHA-$Ca_V1.3$): and either mCherry-$Ca_V1.3$ or GFP-$Ca_V1.2$ used a DNA ratio of 1:1.5. Co-transfections involving GFP-Shank3 or CaMKII, or a combination of GFP-Shank3 and CaMKIIα, with LTCC subunits were performed using a DNA ratio of 3:1:1:1:0.5 (α1:α2δ:FLAG-β2a:CaMKII:Shank3). When GFP-Shank3 or CaMKIIα was expressed individually, empty pCDNA or GFP vector was incorporated to maintain the same overall DNA quantity as co-transfection with GFP-Shank3 and CaMKIIα. For co-immunoprecipitation experiments, HEK293T cells were transfected with a maximum of 10 µg DNA per 10-cm dish and harvested ~48 hours later. For immunostaining experiments, HEK293 cells were transfected with a maximum of 2 µg DNA per well of 6-well plates, and re-plated onto coverslips in 24-well plates ~24 hours later. Coverslips were used for experiments after another 24-36 hours and then fixed.

Co-immunoprecipitation

Transfected HEK 293T cells were lysed and used for co-immunoprecipitation using HA antibody or GFP antibody and magnetic Dynabeads Protein A beads as previously described (Yang *et al.* 2023). Where indicated, lysates were supplemented with 2 mM $CaCl_2$ and/or 1 µM calmodulin (Ca^{2+}/calmodulin), either alone or with 50 µM calmidazolium (Figure S2), prior to incubation.

Western blotting

Co-immunoprecipitation samples were separated on either 7.5% (Figures 2, 10 and S1) or 10% (Figures 3-4, S2, and S7) SDS-PAGE gels, followed by transfer to nitrocellulose membrane as previously described (Yang *et al.* 2023). Membranes were stained with Ponceau-S to confirm protein transfer and loading, and digitally scanned before being incubated in blocking buffer (5% nonfat milk in Tris-buffered saline with 0.1% (v/v) Tween-20 (TBST)) for one hour at room temperature. Primary antibodies (rabbit anti-HA, mouse anti-CaMKII, and rabbit anti-Shank3 were diluted 1:8000; all other primary antibodies were diluted 1:4000) in blocking buffer, and incubated with membranes overnight at 4°C. After washing three times (10 minutes per wash) with TBST, membranes were incubated with IR dye-conjugated secondary antibodies (donkey anti-rabbit 680LT diluted 1:8000 and donkey anti-mouse 800CW diluted 1:4000) in blocking buffer for one hour at room temperature. After two further washes, membranes were scanned using an Odyssey system and images were quantified by Odyssey Image Studio Software. Identically sized rectangles were drawn to select a specific protein band for quantification

across all the lanes on a gel and the background was subtracted using the median background method. Specifically, the area used to compute background is taken from a three-pixel border around top and bottom sides of each rectangle.

HEK cell stimulation and immunocytochemistry

HEK293 cells expressing iHA-$Ca_V1.3$ LTCCs with pcDNA vector or CaMKII (WT or V102E) were pre-incubated in Ca^{2+}-free HEPES buffer (150 mM NaCl, 5 mM KCl, 2 mM $MgCl_2$, 10 mM HEPES pH 7.4, 10 mM Glucose) for 10 min, and then transferred to HEPES buffer supplemented with 10 µM BayK-8644 (BayK) and/or 2.5 mM $CaCl_2$ for 5-10 min. DMSO (0.02% v/v) was added to incubations lacking BayK as a vehicle control. Cells were then fixed using ice-cold 4% paraformaldehyde containing 4% sucrose in 0.1 M Phosphate Buffer (pH 7.4) (4% PFA) for 10 min at room temperature, washed three times (5 min per wash) with PBS, and then permeabilized with PBS containing 0.2% Triton X-100 for 8 min. Subsequently, cells were incubated with blocking solution (1X PBS, 0.1% Triton X-100 (v/v), 2.5% BSA (w/v), 5% Normal Donkey Serum (w/v), 1% glycerol (v/v)) at room temperature for 1 h, then incubated with primary antibodies (rabbit anti-HA diluted 1:1000 and mouse anti-CaMKII diluted 1:2500) in blocking buffer overnight at 4°C. After three washes with PBS containing 0.2% Triton X-100 (10 min each), cells were incubated for one hour at room temperature with secondary antibodies (donkey anti-rabbit Alexa Fluor 647 and donkey anti-mouse Alexa Fluor 488), each diluted 1:2000 in blocking buffer. After three additional washes with PBS, coverslips were mounted on slides using Prolong Gold Antifade Mountant and then stored at 4°C for subsequent imaging.

Total internal reflection fluorescence (TIRF) microscopy and quantification

A Nikon Multi Excitation TIRF microscope with 488 nm and 640 nm solid-state lasers was used as described (Yang *et al.* 2023). The automatic H-TIRF module was used for 488 laser and the manual TIRF module was used for 640 laser. Calibration of the incident angle and focus for achieving TIRF was conducted individually for each module. Images were then acquired using NIS-Elements. Consistency was maintained by using the same exposure time of 80–150 ms for both channels, alongside laser power at 5-8% for 488 nm laser and 10–12% of 640 nm laser. These imaging parameters remained uniform across all cover slips within the same biological replicate. Images were processed in Fiji software (ImageJ, NIH) to quantify cluster density and intensity of surface localized iHA-$Ca_V1.3$, as well as to assess colocalization between iHA-$Ca_V1.3$ and CaMKII. Specifically, cells positive with both iHA and CaMKII signal were selected to be quantified, using freehand selections. These ROIs were then consistently applied to the iHA-$Ca_V1.3$ channel after background subtraction. A threshold for the HA signal was established using the mean intensity of HA signal plus 1.5 times the standard deviation. The “Analyze Particles” function was used to calculate the intensity, area, and count of iHA-$Ca_V1.3$ clusters surpassing the threshold within each ROI. Cluster density was derived by dividing the cluster count by the area of the respective ROI. For colocalization analysis, both CaMKII and HA channels underwent automated thresholding before evaluating the intensity correlation quotient (ICQ). The metric quantifies colocalization on a scale from −0.5 to +0.5, delineating the extent from complete segregation to perfect overlap, as previously described (Li *et al.* 2004; Perfitt *et al.* 2020; Yang *et al.* 2023).

Primary hippocampal neuron cultures and depolarization

Dissociated hippocampal neurons were prepared from E18 Sprague Dawley rat embryos, as previously described (Shanks *et al.* 2010) resulting in cultures containing an approximate 50:50 mix of neurons from male and female embryos. At 14 days in vitro (DIV), neurons on coverslips in 12 well plates were co-transfected using Lipofectamine 2000 (Thermo Fisher Scientific) and 1 µg DNA, in accordance with the manufacturer's directions, to express $Ca_V1.3$/$Ca_V1.2$ α1 subunit with a N-terminal intracellular HA tag (iHA-$Ca_V1.3$) or an extracellular HA tag (sHA-$Ca_V1.3$/sHA-$Ca_V1.2$), FLAG-β2a or -β3, and GFP-nonsense shRNA (nssh) or GFP-CaMKIIα-shRNA and GFP-CaMKIIβ-shRNA (GFP-CaMKII-shRNA) at an α1: β: GFP ratio of 3:1:1.2. After a further 7 days, neurons were pre-incubated in 5K Tyrode's solution (150 mM NaCl, 5 mM KCl, 2 mM $CaCl_2$, 2 mM $MgCl_2$, 10 mM glucose and 10 mM HEPES pH 7.5 (~313 mOsm)) with inhibitors (1 µM TTX, 10 µM APV, and 50 µM CNQX) for 2 hours at 37°C and 5% CO_2 to inhibit the intrinsic neuronal activity. Neurons were then incubated with either 5K or 40K Tyrode's solution (adjusted to 40 mM KCl and 115 mM NaCl, with inhibitors present) for 90 seconds and then quickly fixed in ice-cold 4% PFA for 10 minutes at room temperature, followed by three PBS washes. For surface sHA-Ca_V1 staining, neurons were blocked in non-permeabilizing blocking buffer A (1X PBS, 5% (w/v) bovine serum albumin (Sigma)) for 1 hour. Primary anti-HA antibody (rabbit or mouse, diluted 1:200 in blocking buffer A) was applied overnight at 4°C. After three PBS washes (10 min per wash), neurons were incubated with secondary antibodies (donkey anti-rabbit or anti-mouse Alexa Fluor 647, diluted 1:200 in blocking buffer A) for 1 hour at room temperature. Following three additional washes with PBS, neurons were permeabilized by PBS containing 0.2% Triton X-100 for 8 min, then blocked using blocking buffer B (1X PBS, 0.1% Triton X-100 (v/v), 2.5% BSA (w/v), 5% Normal Donkey Serum (w/v), 1% glycerol (v/v)) for 1 hour. For the following staining for rabbit anti-pCREB (dilution: 1:1000) or mouse anti-CaMKII (dilution: 1:2000), the process was the same as the permeabilized immunostaining in HEK293 cells.

Neuronal imaging and quantification

Neuronal imaging was conducted using Zeiss LSM 880 microscope with a 63x/1.4 Plan-APOCHROMAT oil lens as previously described (Yang *et al.* 2023). Transfected neurons were identified through GFP signals under a binocular lens. Conventional confocal mode was used in Figures 1, 7 and S5. For whole cell imaging (Figures 1C and S5A), Z-stack images were captured with a step size of 0.3 µm and a range of 1.8-2.7 µm. Z-stack images were then processed in Fiji software to create a maximum intensity projection for subsequent analysis. To collect pCREB images, the DAPI channel was used to adjust the focus of nucleus. In Figures 8, 9, 11, and S9 the Airyscan mode was used to maximize sensitivity and resolution for the collection of surface localized sHA-$Ca_V1.2$/sHA-$Ca_V1.3$ and endogenous CaMKII/$Ca_V1.2$ images, collecting single focal plane images (73.51 × 73.51 µm) (Yang *et al*., 2023).

All image quantifications were performed in Fiji software. For endogenous CaMKII analysis, CaMKII signal in the soma was designated as regions of interest (ROIs) in both GFP-positive or -negative neurons. Background was subtracted, and the mean intensities of CaMKII signal in the ROIs were measured. For pCREB analysis, ROIs were assigned based on DAPI signals, and pCREB intensities in these ROIs from GFP-positive or -negative neurons were measured. For LTCC cluster analysis, ROIs were selected based on the GFP channel. Somatic ROIs were selected similarly to that in HEK293 cells, while dendritic ROIs were selected followed rules outlined

previously (Yang *et al.* 2023). Background was then subtracted, sHA signals were thresholded, and the Analyze Particles function was used, as in HEK293 cell analyses. For colocalization between sHA-$Ca_V1.3$ and endogenous $Ca_V1.2$, soma and dendritic ROIs were identified based on GFP signals. Following background subtraction, the average intensities of sHA-$Ca_V1.3$ ($\bar{x}_{1.3}$) and $Ca_V1.2$ ($\bar{x}_{1.2}$) in ROIs were measured. We then defined new ROIs based on sHA staining and separately measured the intensity of sHA-$Ca_V1.3$ and $Ca_V1.2$ in these ROIs. After normalizing sHA signal to $\bar{x}_{1.3}$ and normalizing $Ca_V1.2$ signal to $\bar{x}_{1.2}$, the ratio of normalized $Ca_V1.2$ to normalized sHA intensity in somatic and dendritic ROIs were used as a measure of endogenous $Ca_V1.2$ colocalization with sHA-$Ca_V1.3$. The experimenter was blind to the experimental conditions when analyzing (i/s)HA-$Ca_V1.3$/ sHA-$Ca_V1.2$ clusters in Figures 1, 5-6, and 8-9.

Statistical analysis

All data are shown as mean ± SEM, and sample sizes shown as n refer to the number of cells or independent biological replicates (experiments) as indicated in figure legends. All statistical tests were performed in GraphPad Prism 8 software (GraphPad). Differences were considered significant if $p \leqslant 0.05$. For comparisons between two groups, unpaired Student's t-test (two-tailed) was used. For comparisons between three or more groups with two independent variables, two-way ANOVA followed by the post hoc tests recommended by Prism was used.

Results

Neuronal depolarization increases $Ca_V1.3$ LTCC clustering

We recently reported that Shank3-dependent $Ca_V1.3$ clustering *in vitro* and in HEK293 cells is disrupted by Ca^{2+} (Yang et al, 2023), leading us to hypothesize that depolarization would decrease $Ca_V1.3$ LTCC clustering in cultured hippocampal neurons. Therefore, neurons expressing N-terminal intracellular HA-tagged $Ca_V1.3$ (iHA-$Ca_V1.3$), α2δ, and FLAG-β2a. (DIV21; 7 days post-transfection) were briefly (90 s) depolarized using a well-established 40 mM KCl (40K) protocol in the presence of APV, CNQX and TTX to block NMDA receptors, AMPA receptors, and voltage-dependent sodium channels, respectively. This stimulation paradigm triggers ET coupling in DIV14 hippocampal neurons, as measured by phosphorylation of the CREB transcription factor and by expression of the c-fos immediate early gene (Wheeler *et al.* 2008; Wang *et al.* 2017; Perfitt *et al.* 2020) (Figure 1A). Similarly, the 40K treatment robustly increases nuclear CREB phosphorylation in DIV21 neurons (Figure 1B). In parallel, the 40K treatment significantly increased the intensity and significantly decreased the density of dendritic iHA-$Ca_V1.3$ clusters relative to the control 5K treatment (Figure 1C-D). These results indicate that neuronal depolarization to initiate E-T coupling also induces $Ca_V1.3$ LTCC clustering, inconsistent with our initial hypothesis.

Activated CaMKII assembles complexes containing multiple $Ca_V1.3$ LTCCs

Recruitment of activated CaMKII by the N-terminal domain of $Ca_V1.3$ LTCC α1 subunits is required for E-T coupling (Wheeler *et al.* 2012; Ma *et al.* 2014; Wang *et al.* 2017). Therefore, we tested the hypothesis that activated CaMKII holoenzymes might play a role in $Ca_V1.3$ LTCC clustering by simultaneously binding to multiple α1 subunits. Lysates of HEK293 cells co-expressing iHA- and mCherry-tagged $Ca_V1.3$ α1 subunits, the FLAG-tagged β2a or β3 subunit

and the α2δ subunit, with or without CaMKIIα, were immunoprecipitated using an antibody to the HA epitope. Under standard lysate conditions (with EDTA present: termed basal), the HA antibody co-immunoprecipitated either of the FLAG-tagged β subunits, but negligible amounts of the mCherry-tagged α1 subunit or CaMKIIα. However, Ca^{2+}/calmodulin addition to cell lysates significantly increased the co-immunoprecipitation of mCherry-Ca_V1.3 α1 subunit with the HA-antibody, but only in the presence of co-expressed CaMKIIα (Figure 2A-B). Notably, significant amounts of CaMKIIα co-immunoprecipitated with iHA-Ca_V1.3 only following the addition of Ca^{2+}/calmodulin. These data indicate that CaMKII activation can promote not only CaMKIIα association with Ca_V1.3, as previously observed, but also the assembly of complexes containing multiple Ca_V1.3 α1 subunits.

Prior studies found that activated CaMKIIα also binds to the LTCC β1 and β2a subunits, but not to β3 or β4 subunits (Grueter *et al.* 2008; Abiria & Colbran 2010). We found that co-expression of FLAG-β2a substantially enhanced the co-immunoprecipitation of mCherry-Ca_V1.3 and CaMKIIα with iHA-Ca_V1.3 in the presence of Ca^{2+}/calmodulin relative to the amounts co-immunoprecipitated with FLAG-β3 co-expression, even though the cells expressed higher levels of FLAG-β3 than FLAG-β2a, as measured by the anti-FLAG immunoblot (Figure 2A-B). These data indicate that β2a subunits can further enhance the assembly of complexes containing activated CaMKII and multiple Ca_V1.3 α1 subunits.

Requirements for CaMKII-dependent Ca_V1.3 complex assembly

To determine whether both Ca^{2+} and calmodulin are required for CaMKIIα-dependent formation of multimeric Ca_V1.3 complexes, we tested whether Ca^{2+} alone or calmodulin alone would support complex formation in HEK cell lysates using the co-immunoprecipitation assay. Consistent with Figure 2A, negligible levels of mCherry-Ca_V1.3 associated with iHA-Ca_V1.3 in the absence of CaMKIIα under any conditions. Moreover, in contrast to the effect of adding both Ca^{2+} and calmodulin, neither Ca^{2+} nor calmodulin alone enhanced the co-immunoprecipitation of mCherry-Ca_V1.3 with iHA-Ca_V1.3, even in the presence of CaMKIIα (Figure 3A-B). A similar result was obtained in the presence of FLAG-β3 (Figure S1). To further investigate the Ca^{2+}/calmodulin requirement, we tested the effects of calmidazolium (50 μM), a widely used calmodulin antagonist, on co-immunoprecipitations from HEK293T cell lysates containing iHA-Ca_V1.3, mCherry-Ca_V1.3, α2δ, FLAG-β2a, and CaMKIIα (Figure S2A). Calmidazolium essentially abrogated the Ca^{2+}/calmodulin-dependent association of mCherry-Ca_V1.3 and CaMKIIα with iHA-Ca_V1.3 (Figure S2B). Taken together, these data indicate that the combined actions of both Ca^{2+} and calmodulin are required for CaMKIIα-dependent formation of multimeric Ca_V1.3 complexes.

CaMKII-dependent assembly of multi-Ca_V1.3 complexes in the presence of Shank3

We previously reported that basal Shank3-dependent assembly of multimeric Ca_V1.3 complexes is disrupted by Ca^{2+}/calmodulin (Yang *et al.* 2023). Therefore, we investigated the impact of Shank3 on Ca^{2+}/calmodulin- and CaMKII-dependent assembly of Ca_V1.3 complexes. Lysates of HEK293T cells co-expressing iHA-Ca_V1.3, mCherry-Ca_V1.3, α2δ, and FLAG-β2a with CaMKIIα or GFP-Shank3, or both CaMKIIα and GFP-Shank3, were immunoprecipitated using HA antibodies under basal conditions (EDTA) or following Ca^{2+}/calmodulin addition (Figure 4A). As seen

previously, Shank3 alone associated with iHA-$Ca_V1.3$ enhancing co-immunoprecipitation of mCherry-$Ca_V1.3$ α1 subunits under basal (EDTA) conditions, but not following Ca^{2+}/calmodulin addition (Yang *et al.* 2023). Conversely, CaMKIIα co-expression enhanced the association of mCherry-$Ca_V1.3$ and FLAG-β2a with iHA-$Ca_V1.3$ only after Ca^{2+}/calmodulin addition, as seen in Figure 2. However, in the presence of both CaMKIIα and GFP-Shank3, substantially more mCherry-$Ca_V1.3$ co-immunoprecipitated with iHA-$Ca_V1.3$ from basal (EDTA) cell lysates, even though there were no significant changes in the levels of co-precipitated iHA-$Ca_V1.3$ or GFP-Shank3 (relative to lysates lacking CaMKIIα), and no significant co-precipitation of inactive CaMKII (Figure 4B). Moreover, the addition of Ca^{2+}/calmodulin to cell lysates containing CaMKIIα and GFP-Shank3 significantly increased the recruitment of CaMKIIα into the iHA-$Ca_V1.3$ complex in parallel with an increased precipitation of iHA-$Ca_V1.3$ itself, but there was no further increase in the levels of co-precipitated mCherry-$Ca_V1.3$. Moreover, similar levels of GFP-Shank3 were present in iHA-$Ca_V1.3$ complexes in the presence of CaMKIIα. Notably, the ratio of mCherry-$Ca_V1.3$ to iHA-$Ca_V1.3$ was significantly higher under both EDTA and Ca^{2+}/calmodulin conditions in the presence of both GFP-Shank3 and CaMKIIα than it was under basal conditions with GFP-Shank3 alone, or Ca^{2+}/calmodulin conditions with CaMKIIα alone (Figure 4). These findings indicate that, in the presence of both Shank3 and CaMKIIα, Shank3 is predominantly responsible for the assembly of multi-$Ca_V1.3$ complexes under basal conditions, but that in the presence of CaMKIIα, Shank3 is retained following the addition of Ca^{2+}/calmodulin, further enhancing $Ca_V1.3$ LTCC complex formation.

CaMKIIα and Ca^{2+} influx enhances plasma membrane $Ca_V1.3$ clustering in intact cells

We next tested the hypothesis that assembly of complexes containing multiple $Ca_V1.3$ α1 subunits by activated CaMKII enhances the clustering of cell surface $Ca_V1.3$ LTCCs in intact HEK293 cells. We co-expressed iHA-$Ca_V1.3$, α2δ, and FLAG-β2a subunits with or without wild type CaMKIIα. Cells were pre-incubated in a Ca^{2+}-free HEPES buffer for 10 minutes and then in HEPES buffer with or without BayK (10 µM), an LTCC agonist, in the presence or absence of 2.5 mM Ca^{2+} for 5-10 minutes, prior to fixation and permeabilization. After immunolabeling for HA and CaMKIIα, we used total internal reflection fluorescence (TIRF) microscopy to detect immunofluorescent labels residing within ~100 nm of the cover slip. As seen previously (Yang *et al.* 2023), iHA-$Ca_V1.3$ was readily detected on, or near, the cell surface under all experimental conditions (Figure 5A), and we quantified the intensity (Figure 5B) and density (Figure 5C) of the puncta. In the absence of co-expressed CaMKIIα, the addition of Ca^{2+} and/or BayK had no significant effect on the iHA-$Ca_V1.3$ puncta intensity. Co-expression of CaMKIIα significantly, if modestly, increased the puncta intensity in the absence of Ca^{2+} and/or BayK. However, inclusion of both Ca^{2+} and BayK significantly increased the iHA-$Ca_V1.3$ puncta intensity. Moreover, CaMKIIα co-expression modesty reduced iHA-$Ca_V1.3$ cluster density independent of the cell treatment conditions (Figures 5 and S3). These data indicate that Ca^{2+} influx via $Ca_V1.3$ LTCCs induces $Ca_V1.3$ α1 subunit clustering in the plasma membrane of intact HEK293 cells via a CaMKII-dependent mechanism.

To further investigate the requirements for CaMKII- and Ca^{2+}/BayK-dependent increases in iHA-$Ca_V1.3$ puncta intensity in the plasma membrane, we co-expressed of iHA-$Ca_V1.3$ LTCCs with either WT CaMKIIα (CaMKII-WT) or a V102E CaMKIIα mutant (CaMKII-V102E), which selectively

disrupts binding to the N-terminal domain of $Ca_V1.3$ α1 subunits (Wang *et al.* 2017). HEK293 cells were treated with either Ca^{2+}-free HEPES buffer (0 Ca^{2+}) or HEPES buffer supplemented with 2.5 mM Ca^{2+} and BayK (Figures 6 and S4). As seen in Figure 5, in the presence of CaMKII-WT the intensity of surface-localized iHA-$Ca_V1.3$ clusters was significantly increased following Ca^{2+}/BayK incubation, in parallel with a decrease in cluster density (Figures 6B, S4A, and S4B). However, Ca^{2+}/BayK-induced changes in iHA-$Ca_V1.3$ clustering were not observed in cells expressing the CaMKII-V102E mutant. Concurrently, we assessed CaMKIIα colocalization with iHA-$Ca_V1.3$ using the ICQ method (Figures 6B and S4C). Under basal conditions, ICQ scores for cells co-expressing CaMKII-WT (~0.25) and CaMKII-V102E (~0.23) were similar. However, following the Ca^{2+}/BayK incubation, there was a significant increase of the ICQ score in cells expressing CaMKII-WT (~0.31), that was not detected in cells co-expressing CaMKII-V102E. Taken together, these findings indicate that binding of activated CaMKII to the $Ca_V1.3$ N-terminal domain is required for $Ca_V1.3$ clustering in the plasma membrane of HEK293 cells.

Activity-dependent clustering of $Ca_V1.3$ in hippocampal neurons requires endogenous CaMKII

To test the role of CaMKII in neuronal $Ca_V1.3$ LTCC clustering, we transfected hippocampal neurons at DIV14 to express $Ca_V1.3$ tagged with an extracellular HA epitope (sHA-$Ca_V1.3$) and FLAG-β2a with either a nonsense shRNA (nssh) or specific shRNAs targeting CaMKIIα and CaMKIIβ (CaMKII-sh) (both with a soluble GFP marker). Neurons expressing control nssh contained somatic and dendritic pools of CaMKII, with no significant change in intensity compared to adjacent non-transfected neurons (Figure S5A-B). In contrast, the intensity of CaMKII staining in neurons expressing the CaMKII-sh was significantly reduced by about 77% relative to nearby non-transfected neurons (Figure S5B-B'). Thus, the shRNAs effectively suppressed CaMKII expression under the current experimental conditions.

To assess the biological impact of sHA-$Ca_V1.3$ over-expression in neurons and confirm the role of CaMKII under these conditions, we depolarized neurons using 40mM KCl for 90 seconds (as in Figure 1A), fixed the neurons and then labeled surface-localized sHA-$Ca_V1.3$. Neurons were then permeabilized and labeled for Ser133 phosphorylation of CREB (pCREB) (Figure 7A). The depolarization of neurons expressing sHA-$Ca_V1.3$ with control nssh shRNA robustly increased CREB phosphorylation, and to a slightly, but significantly, greater extent compared to nearby non-transfected neurons (Figures 7B and S6A). However, depolarization of neurons expressing sHA-$Ca_V1.3$ and the CaMKII-sh shRNA resulted in significantly ~43% lower levels of nuclear CREB phosphorylation compared to nearby non-transfected neurons (Figures 7C and S6B). Taken together, these data indicate that E-T coupling in DIV21 neurons overexpressing sHA-$Ca_V1.3$ was partially CaMKII-dependent, as seen in DIV14 neurons expressing only endogenous LTCCs (Wheeler *et al.* 2008; Wang *et al.* 2017).

Next, we collected super-resolution images of surface-expressed sHA-$Ca_V1.3$ LTCCs using the Airyscan mode of a Zeiss LSM880 microscope and quantified sHA-$Ca_V1.3$ puncta intensity and density with or without neuronal depolarization (Wu & Hammer 2021; Yang *et al.* 2023). In neurons expressing control nssh shRNA, depolarization significantly increased sHA-$Ca_V1.3$ puncta intensity in both the soma and dendrites compared to 5K treatment (Figure 8A-C), consistent with changes in total iHA-$Ca_V1.3$ puncta observed in Figure 1B. However, in neurons

expressing CaMKII-sh shRNA, depolarization resulted in a significant decrease in sHA-$Ca_V1.3$ puncta intensity in both the soma and dendrites (Figure 8D-F). There was no significant effect of depolarization on the density of somatic or dendritic puncta with or without CaMKII knockdown (Figure 8B-C and 8E-F). Taken together, these data indicate that CaMKII is important for increased clustering of surface localized $Ca_V1.3$ LTCCs following a brief depolarization under conditions that initiate E-T coupling.

CaMKII-dependent clustering of neuronal $Ca_V1.2$ following depolarization

We previously showed that the N-terminal domain of the closely related $Ca_V1.2$ LTCC α1 subunit also contains a conserved CaMKII-binding motif that binds activated CaMKII (Wang *et al.* 2017). Therefore, we tested the hypothesis that depolarization also regulates the surface distribution of sHA-$Ca_V1.2$ α1 subunits using a similar approach (Figure 9). In neurons expressing the control nssh shRNA, depolarization significantly increased the intensity of sHA-$Ca_V1.2$ puncta in both the soma and dendrites, without affecting puncta density (Figure 9B-C). However, puncta intensity was significantly decreased in the soma, but not the dendrites of neurons expressing CaMKII-sh shRNAs following depolarization (Figure 9E-F). Depolarization also increased sHA-$Ca_V1.2$ puncta density in the soma, but not the dendrites, of CaMKII-sh-expressing neurons. Taken together, these data show that neuronal depolarization induces a CaMKII-dependent increase in the clustering of $Ca_V1.2$ LTCCs, similar that observed for $Ca_V1.3$.

CaMKII-dependent assembly of $Ca_V1.2$-$Ca_V1.3$ complexes *in vitro*.

Since activated CaMKIIα can assemble complexes containing multiple $Ca_V1.3$ α1 subunits, and CaMKII is required for depolarization-induced $Ca_V1.2$ and $Ca_V1.3$ cluster formation in neurons, we hypothesized that CaMKII can assemble protein complexes containing both $Ca_V1.2$ and $Ca_V1.3$. To test this hypothesis, lysates of HEK293T cells co-expressing iHA-$Ca_V1.3$, GFP-$Ca_V1.2$, α2δ, and FLAG-β2a with or without wild type CaMKIIα were immunoprecipitated using an HA antibody under basal conditions (with EDTA) or following Ca^{2+}/calmodulin addition (Figure 10A). Under basal conditions, minimal levels of GFP-$Ca_V1.2$ were detected in HA immune complexes in the absence or presence of co-expressed CaMKIIα. However, the addition of Ca^{2+}/calmodulin to lysates containing CaMKIIα significantly increased the levels of GFP-$Ca_V1.2$, CaMKIIα and FLAG-β2a in the iHA-$Ca_V1.3$ complex (Figure 10B). In lysates lacking CaMKIIα, the addition of Ca^{2+}/calmodulin induced a small, but significant increase in the association of GFP-$Ca_V1.2$ with iHA-$Ca_V1.3$. In a second series of experiments, we found that the CaMKIIα-V102E mutation, which disrupts CaMKIIα binding to both $Ca_V1.3$ and $Ca_V1.2$ (Figure S7), failed to support the assembly of $Ca_V1.2$-$Ca_V1.3$ complexes in the presence of Ca^{2+}/calmodulin (Figure 10C-D). Taken together, these data support the hypothesis that direct interactions of the activated CaMKIIα catalytic domain with N-terminal domains of the LTCC α1 subunits can assemble complexes containing $Ca_V1.2$ and $Ca_V1.3$ α1 subunits *in vitro*.

The colocalization of $Ca_V1.3$ and $Ca_V1.2$ LTCCs in cultured neurons

We next examined the potential co-clustering of $Ca_V1.3$ and $Ca_V1.2$ LTCCs in cultured hippocampal neurons, and investigated the impact of knocking down CaMKII expression. Neurons were co-transfected with sHA-$Ca_V1.3$, FLAG-β2a, and either nssh or CaMKII-sh at DIV 14, and after 7 days (DIV21) they were depolarized with 40mM KCl for 90 seconds and fixed.

Immunostaining was performed for the sHA tag (without permeabilization) on $Ca_V1.3$ and endogenous $Ca_V1.2$ (following permeabilization) (Figure 11A-B). Regions of interest (ROIs) were defined based on the sHA-$Ca_V1.3$ signal and the amount of endogenous $Ca_V1.2$ staining within each ROI was quantified. The ratios of endogenous $Ca_V1.2$ intensity to sHA-$Ca_V1.3$ intensity within each ROI were quantified separately in the soma (Figure 11C and Supplemental Figure S8A) and the dendrites (Figure 11D and Figure S8B). This approach allows us to quantify $Ca_V1.2$ signals derived predominantly from transfected neurons and not nearby non-transfected cells. Thus, the intensity ratio is proportional to the degree of co-localization between $Ca_V1.2$ and sHA-$Ca_V1.3$. We found that the e$Ca_V1.2$/sHA-$Ca_V1.3$ staining ratio was relatively low in both the soma and dendrites under basal (5K treatment) conditions (mean normalized to 1.0), and was unaffected by CaMKII knockdown. However, depolarization resulted in a significant increase in the e$Ca_V1.2$/sHA-$Ca_V1.3$ staining ratio in the soma and dendrites of neurons expressing nssh but not following CaMKII knockdown. Since depolarization increases the clustering of both $Ca_V1.3$ and $Ca_V1.2$ individually, we interpret the depolarization-induced increased $Ca_V1.2$ to sHA-$Ca_V1.3$ staining ratio as representing co-clustering of $Ca_V1.2$ with sHA-$Ca_V1.3$. Furthermore, closer qualitative examination of these images indicated that a subfraction of the endogenous $Ca_V1.2$ appeared to be localized to dendritic spines, whereas sHA-$Ca_V1.3$ staining, and the co-clustered channels were mostly localized to dendritic shafts (Figure S9). Overall, these data demonstrate that neuronal depolarization induces the plasma membrane co-clustering of $Ca_V1.2$ with $Ca_V1.3$ via a CaMKII-dependent mechanisms.

Discussion

This research provides novel insights into molecular mechanisms that contribute to clustering neuronal LTCCs that are major initiators of E-T coupling. Using a series of co-immunoprecipitation and fluorescence microscopy experiments, we found that CaMKII assembles homo- or hetero-meric $Ca_V1.3$ or $Ca_V1.2$ LTCC complexes in an activity dependent manner *in vitro* and in the plasma membrane of HEK cells. This clustering is facilitated by co-expression of the CaMKII-binding LTCC β2a subunit relative to the β3 subunit. Additionally, clustering is disrupted by a V102E mutation within CaMKII catalytic domain. We found that neuronal depolarization increased the clustering of both $Ca_V1.2$ and $Ca_V1.3$, as well as the co-clustering of these channels, and that shRNA-mediated knockdown of CaMKII expression impaired (co-)clustering. Since these depolarization conditions increase nuclear CREB phosphorylation and c-fos expression in neurons, and these increases are blocked by LTCC antagonists or by disrupting CaMKII interactions with the LTCC, the current findings suggest that CaMKII-dependent clustering of LTCCs is linked to E-T coupling.

Clustering of L-type Ca^{2+} channels

It is well established that LTCCs have a propensity to form clusters in the plasma membrane. These clusters can contain other ion channels and modulate action potentials in neurons and neuroendocrine cells (Vivas *et al.* 2017; Cox 2014; Marcantoni *et al.* 2010; Vandael *et al.* 2010; Plante *et al.* 2021). For example, neuronal plasma membrane clustering of $Ca_V1.2$ with voltage-gated $K_V2.1$ potassium channels in the soma and proximal dendrites facilitates additional interactions with ryanodine receptors (RyRs) in the endoplasmic reticulum membrane,

facilitating Ca^{2+} release from the endoplasmic reticulum (Vierra *et al.* 2019). Disruption of $Ca_V1.2$-$K_V2.1$ clustering interferes with E-T coupling (Vierra *et al.* 2021). LTCCs can form clusters containing an average of approximately eight α1 subunits in both adult ventricular myocytes ($Ca_V1.2$) and cultured hippocampal neurons ($Ca_V1.3$) (Dixon *et al.* 2015; Moreno *et al.* 2016). Notably, this clustering facilitates the functional coupling of $Ca_V1.2$ and $Ca_V1.3_S$ (isoform with a short C-terminal domain), enhancing Ca^{2+} influx following depolarization (Fallon *et al.* 2009; Dixon *et al.* 2015; Moreno *et al.* 2016). Interaction of the two lobes of Ca^{2+}/calmodulin with α1 subunit C-terminal domains appears to be important for this functional coupling (Moreno *et al.* 2016; Dixon *et al.* 2015). However, the $Ca_V1.3_L$ isoform used in the current studies, which contains the full-length C-terminal domain including the Ca^{2+}/calmodulin-binding site, forms similar sized clusters but without any functional coupling. Taken together, these prior studies indicate that the molecular basis for physical clustering and functional coupling of LTCCs remains poorly understood.

Proteins that interact with the LTCC intracellular domains also may play a role in clustering, particularly if these proteins dimerize or multimerize. For example, the PDZ domain of Shank3, a synaptic scaffolding protein, directly interacts with the C-terminal motif of $Ca_V1.3_L$ to facilitate synaptic surface expression (Zhang *et al.* 2005; Zhang *et al.* 2006). Shank3 homo-multimerizes via interactions between C-terminal SAM domains (Sheng & Kim 2000), and we recently reported that Shank3 clusters multiple $Ca_V1.3$ LTCCs under basal (low Ca^{2+}) conditions *in vitro*, in HEK293 cells, and in cultured hippocampal neurons (Yang *et al.* 2023). However, knockdown of Shank3 expression had no effect on the clustering of neuronal $Ca_V1.2$ LTCCs, which cannot bind to the Shank3 PDZ domain. Interestingly, we found that Ca^{2+}/calmodulin disrupts Shank3 dependent clustering of $Ca_V1.3$ *in vitro* and in HEK293 cells in parallel with the dissociation of Shank3 from the complex (Yang *et al.* 2023), in contrast to our current findings showing neuronal depolarization enhances LTCC clustering.

Activity-dependent clustering of LTCCs by CaMKII

CaMKII was reported to interact with the C- and N-terminal domains of the LTCC $Ca_V1.2$ α1 subunit to modulate their biophysical properties or intracellular trafficking, respectively (Hudmon *et al.* 2005; Simms *et al.* 2015). We recently identified an "RKR" motif in the N-terminus of the $Ca_V1.3$ α1 subunits that selectively binds to activated CaMKII and showed that this interaction is required for neuronal LTCC-dependent E-T coupling (Wang *et al.* 2017). Notably, the RKR motif is conserved in the N-terminal domain of $Ca_V1.2$ but is not contained within the N-terminal CaMKII-binding domain identified by Simms et al (2015). While reasons for these discrepancies are unclear, the current data provide new insights into the role of CaMKII binding to N-terminal domains of both $Ca_V1.2$ and $Ca_V1.3$. A combination of *in vitro* co-immunoprecipitation assays, fluorescence microscopy in heterologous cells, and shRNA-knockdown of CaMKII expression in cultured hippocampal neurons revealed that activated CaMKII is responsible for clustering multiple $Ca_V1.3$ and/or $Ca_V1.2$ LTCCs in response to neuronal depolarization. Notably, a V102E mutation in the catalytic domain of CaMKIIα, which disrupts interactions with the N-terminal domain RKR motif and interferes with E-T coupling, prevents activity-dependent LTCC clustering. These data indicate that clustering is due to

interactions of multiple activated CaMKII catalytic domains within a single CaMKII holoenzyme with the N-terminal domains of distinct LTCC α1 subunits.

β2a subunit facilitate CaMKII mediated LTCC clustering

Four variants of the β auxiliary subunits play unique roles in modulating the biophysical properties of LTCCs and their trafficking to the plasma membrane (Buraei & Yang 2010; Dolphin 2003; Jarvis & Zamponi 2007). Our biochemical data indicate that LTCC β subunits may also modulate CaMKII-dependent LTCC clustering. We previously reported that activated CaMKII selectively binds to the β1 and β2a subunits, but not to β3 or β4 subunits (Grueter *et al.* 2008), enhancing CaMKII association with $Ca_V1.2$ LTCCs (Abiria & Colbran 2010). Furthermore, mutation of β2a to prevent CaMKII binding also disrupts CaMKII-dependent facilitation of $Ca_V1.2$ LTCCs in cardiomyocytes (Koval *et al.* 2010). Although the present biochemical studies demonstrated the Ca^{2+}/calmodulin and CaMKII-dependent assembly of multi-LTCC complexes in the presence of either β2a or β3 subunits, complex assembly was substantially enhanced with β2a relative to β3 (Figure 2). It will be interesting to investigate the potential role of β2a palmitoylation in LTCC (co-)clustering, since this modification has been show to enhance plasma membrane targeting of $Ca_V1.2$ and $Ca_V1.3$ (Gao *et al.* 1999).

Modulation of LTCC clustering by Shank3

Shank3 also directly interacts with both $Ca_V1.3$ and activated CaMKII and disruption of either the Shank3-$Ca_V1.3$ or the Shank3-CaMKII interactions interferes with LTCC-mediated E-T coupling in cultured hippocampal neurons (Perfitt *et al.* 2020). Moreover, we found that Shank3 enhances both the formation of multimeric $Ca_V1.3$ complexes under basal conditions *in vitro*, and the clustering of $Ca_V1.3$ in HEK293 cells, but the formation of these $Ca_V1.3$ complexes/clusters is disrupted by Ca^{2+}/calmodulin *in vitro* or by Ca^{2+} influx via the LTCC in HEK293 cells (Yang *et al.* 2023). Consistent with these observations we previously reported that suppression of Shank3 expression in cultured hippocampal neurons decreased the basal clustering of $Ca_V1.3$ LTCCs, but had no effect on basal clustering of $Ca_V1.2$ (which does not bind to Shank3). Given these prior findings, we were initial surprised that depolarization enhanced neuronal $Ca_V1.3$ clustering (Figure 1), leading us to uncover critical roles for CaMKII in depolarization-induced clustering of both $Ca_V1.3$ and $Ca_V1.2$ reported here. Moreover, we found that the suppression of neuronal CaMKII expression uncovered a significant depolarization-induced decrease in $Ca_V1.3$ clustering (Figure 8D-E), as might be predicted based on our prior *in vitro* and HEK293 studies of the $Ca_V1.3$-Shank3 interaction. These observations raise questions about the role of Shank3 in $Ca_V1.3$ clustering following depolarization, especially in CaMKII-expressing neurons.

Our *in vitro* experiments revealed that the formation of multimeric iHA-$Ca_V1.3$ complexes under basal conditions is surprisingly enhanced in the presence of both CaMKII**α** and Shank3 compared to the presence of either CaMKII**α** or Shank3 alone (Figure 4), even though inactive CaMKII**α** is not associated with immunoprecipitated basal complexes in the presence or absence of Shank3. Ca^{2+}/calmodulin addition to cell lysates containing both CaMKIIα and Shank3 enhanced CaMKIIα association with iHA-$Ca_V1.3$ complexes to a greater extent than observed when only CaMKIIα is present. Moreover, Shank3 remained associated with $Ca_V1.3$ complexes following the addition of Ca^{2+}/calmodulin in the presence of CaMKIIα, in contrast to

the dissociation of Shank3 that was observed in the absence of CaMKIIα. Taken together, these observations indicate that Shank3 and CaMKII have complex interacting roles in modulating the formation of multimeric $Ca_V1.3$ complexes under basal conditions and following CaMKII activation. However, the precise biochemical mechanisms underlying these effects are unclear and further studies are required to more fully investigate cooperative roles of Shank3 and CaMKII in modulating LTCC clustering.

Potential roles of $Ca_V1.2$ and $Ca_V1.3$ co-clustering

As noted above, homomeric clustering of $Ca_V1.2$ and $Ca_V1.3$ α1 subunits enhances functional coupling between the channels (Dixon *et al.* 2015; Moreno *et al.* 2016), and LTCC clustering with other ion channels has important physiological roles (Vivas *et al.* 2017; Cox 2014; Marcantoni *et al.* 2010; Vandael *et al.* 2010; Plante *et al.* 2021; Vierra *et al.* 2019; Vierra *et al.* 2021). $Ca_V1.2$ and $Ca_V1.3$ are the most closely homologous LTCC α1 subunits, and are co-expressed at varying ratios in neurons across many brain regions (Striessnig *et al.* 2014), where they appear to be preferentially localized to the soma, dendritic shafts, and dendritic spines (Folci *et al.* 2018; Stanika *et al.* 2016). Under some conditions, E-T coupling is mediated by a wave of dendritic LTCC activation, initiated at dendritic spines and propagating to the soma, that appears to be independent of sodium channel activity (Wild *et al.* 2019). It is remarkable that loading neurons with BAPTA to chelate intracellular Ca^{2+} blocks LTCC-dependent E-T coupling, but E-T coupling is preserved in neurons loaded with the slow Ca^{2+} chelator, EGTA (Deisseroth *et al.* 1996; Ma *et al.* 2012). These observations suggest that E-T coupling can be initiated by Ca^{2+} signaling events in a nanodomain in close proximity to the LTCC, that can be blocked only by BAPTA, without requiring global Ca^{2+} increases, that are blocked by both BAPTA and EGTA. Subsequent studies showed that CaMKII recruitment to the LTCC Ca^{2+} signaling nanodomain is required to initiate E-T coupling (Wheeler *et al.* 2008; Ma *et al.* 2014; Wang *et al.* 2017).

$Ca_V1.2$ and $Ca_V1.3$ are highly homologous, yet have distinct biophysical properties and can be regulated via distinct mechanisms, yet it has proven challenging to identify unique physiological roles for these two channels. Perhaps most significantly, $Ca_V1.3$ is more sensitive to membrane depolarization than $Ca_V1.2$, presumably underlying previous observations that $Ca_V1.3$ channels play a more dominant role in initiating neuronal E-T coupling in response to modest membrane depolarization (20-45 mM KCl), whereas the generally more abundant $Ca_V1.2$ channels are dominant only with more robust depolarization (90 mM KCl) (Zhang *et al.* 2006). The combined use of transgenic mouse manipulations with administration of LTCC agonists or blockers *in vivo* revealed important roles for both $Ca_V1.3$ and $Ca_V1.2$ in neuronal E-T coupling, although the two channels have relatively dominant roles in E-T coupling in distinct brain regions (Hetzenauer *et al.* 2006). Our studies found that a brief (90 s) modest (40 mM KCl) depolarization that initiates E-T coupling increases endogenous $Ca_V1.2$ co-localization with over-expressed plasma membrane sHA-$Ca_V1.3$ in hippocampal neurons. Although we could not differentiate surface expressed vs. intracellular pools of endogenous $Ca_V1.2$ in the co-clusters, these data suggest that $Ca_V1.3$ and $Ca_V1.2$ channels may “collaborate” to regulate downstream signaling under some circumstances.

We posit that co-clustering facilitates the collaboration of $Ca_V1.3$-$Ca_V1.2$ channels to initiate E-T coupling. We suggest that more modest (physiological) depolarizing stimuli selectively activate $Ca_V1.3$ (since it is a more sensitive voltage-sensor) to trigger an initial influx of Ca^{2+}. This Ca^{2+} influx activates CaMKII, resulting in its recruitment to an initial $Ca_V1.3$ LTCC nanodomain that reinforces CaMKII activation. Activated dodecameric holoenzymes bound to $Ca_V1.3$ then serve as scaffolding proteins to recruit $Ca_V1.2$, forming multimeric $Ca_V1.2$-$Ca_V1.3$ co-clusters. LTCC activation within the larger LTCC co-cluster would create more substantial Ca^{2+} signals (higher concentrations and/or larger spread) that might be required to initiate transmission of a long-range signal from dendrites to the nucleus to activate transcriptional responses (Figure 12). Clearly, much more work will be needed to test various aspects of this proposed model.

Acknowledgements
This work was supported by Vanderbilt University and an endowed Louise B. McGavock Chair to R.J.C. Imaging experiments and data analysis were performed in part through the use of the Vanderbilt Cell Imaging Shared Resource (supported by National Institutes of Health Grants CA68485, DK20593, DK58404, DK59637, and EY08126). The content is solely the responsibility of the authors and does not necessarily represent the official views of the National Institutes of Health.

Conflict of interest disclosure
The authors declare that they have no competing interests.

Author contributions
Q.Y. and R.J.C designed research; Q.Y. and D.L. performed biochemistry experiments; Q.Y. performed imaging experiments; L.H. prepared rat hippocampal neuronal cultures; Q.Y. and L.H. performed neuron depolarization experiments; Q.Y. and D.L. analyzed data; drafts of the manuscript were originally written by Q.Y. and then edited by R.J.C. All authors participated in the discussion, revision, and approval of the final manuscript.

Key resources table		
REAGENT or RESOURCE	**SOURCE**	**IDENTIFIER or GENBANKACCESSION#**
Antibodies		
Rabbit anti-Phospho-CREB (Ser133) (87G3)	Cell Signaling	Cat# 9198
rabbit monoclonal anti-HA (C29F4)	Cell Signaling	Cat# 3724S
mouse monoclonal anti-HA.11	BioLegend	Cat# 901502
mouse monoclonal anti-mCherry (1C51)	Novus Biologicals	Cat# NBP-96752
mouse monoclonal anti-Flag M2	Sigma	Cat# F3165

mouse monoclonal anti-CaMKIIα (6G9)	Invitrogen	Cat# MA1-048
p-CaMKIIα (Thr 286)-R	Santa Cruz	Cat# sc-12886-R
rabbit monoclonal anti-Shank3 (D5K6R)	Cell Signaling	Cat# 64555
mouse anti-GFP (clone 1C9A5)	Vanderbilt Antibody and Protein Resource	
rabbit anti-GFP	Invitrogen	Cat# A11122
mouse anti-CaV1.2	Almone	Cat# ACC003
IR dye-conjugated donkey anti-mouse 800CW	LI-COR Biosciences	Cat# 926–32212
IR dye-conjugated donkey anti-rabbit 680LT	LI-COR Biosciences	Cat# 926–68023
donkey anti-mouse Alexa Fluor 647	Thermo Fisher Scientific	Cat# A-31571
donkey anti-mouse Alexa Fluor 546	Thermo Fisher Scientific	Cat# A-10036
donkey anti-mouse Alexa Fluor 488	Thermo Fisher Scientific	
donkey anti-rabbit Alexa Fluor 647	Thermo Fisher Scientific	
donkey anti-rabbit Alexa Fluor 546	Thermo Fisher Scientific	Cat# A-10040
Purified proteins		
calmodulin	homemade	
CaMKIIα	homemade	
DNA constructs		
CaV1.3 α1	Rattus norvegicus	AF370010
pCGNH (N-terminal HA tag)	(X. Wang et al., 2017)	
pmCherry-C1	Xiaohan Wang created in the lab (X. Wang et al., 2017)	
pCGNO (external HA tag)	This construct was created according to (Altier et al., 2002)	
CaV α2δ	Oryctolagus cuniculus	M21948
pCDNA	(X. Wang et al., 2017)	
CaV β3	Rattus norvegicus	M88751
pCMV-Flag	(X. Wang et al., 2017)	
CaV β2a	Rattus norvegicus	M80545
pCMV-Flag	(X. Wang et al., 2017)	
CaMKIIα (WT and V102E)	Mus musculus	X14836.1
pCDNA	(X. Wang et al., 2017)	

Shank3	Rattus norvegicus	a gift from Dr. Craig Garner
EGFP-C1	(Perfitt et al., 2020)	
CaV1.2 α1	Rattus norvegicus	a gift from Dr. Gerald Zamponi
EGFP-C1	Xiaohan Wang created in the lab	
pCGNO (external HA tag)*	Xiaohan Wang created in the lab	
pLL3.7 (construct expressing shRNA)	(Dittgen et al., 2004)	a gift from Dr. Luk Van Parijs
Nonsense shRNA	(Boudkkazi et al., 2014)	5'-TCGCTTGGGCGAGAGTAAG-3'
CaMKIIα shRNA	(Wheeler et al., 2008)	5'-GAATGATGGCGTGAAGGAA-3'
CaMKIIβ shRNA	(Wheeler et al., 2008)	5'-GAGTATGCAGCTAAGATCA-3'
Chemicals		
TTX	TOCRIS	Cat# 1078
CNQX	TOCRIS	Cat# 1045
APV	TOCRIS	Cat# 0106
Bay K8644	TOCRIS	Cat# 1544
DMSO	Sigma	D8418
Calmidazolium chloride	TOCRIS	Cat# 2561
Cell lines		
Human: HEK293T	ATCC	CRL-3216
Human: HEK293	ATCC	CRL-1573
*After these studies were mostly completed, we detected a mutation in the cDNA encoding sHA-CaV1.2 which results in a Lys2055 mutation to Asn, 86 amino acids away from the C-terminus.		

Reference

Abiria, S. A. and Colbran, R. J. (2010) CaMKII associates with CaV1.2 L-type calcium channels via selected beta subunits to enhance regulatory phosphorylation. *J Neurochem* **112,** 150-161.

Birnbaumer, L., Qin, N., Olcese, R., Tareilus, E., Platano, D., Costantin, J. and Stefani, E. (1998) Structures and functions of calcium channel beta subunits. *J Bioenerg Biomembr* **30,** 357-375.

Buraei, Z. and Yang, J. (2010) The ß subunit of voltage-gated Ca2+ channels. *Physiol Rev* **90,** 1461-1506.

Cai, Q., Zeng, M., Wu, X., Wu, H., Zhan, Y., Tian, R. and Zhang, M. (2021) CaMKIIα-driven, phosphatase-checked postsynaptic plasticity via phase separation. *Cell Res* **31,** 37-51.

Cox, D. H. (2014) Modeling a Ca(2+) channel/BKCa channel complex at the single-complex level. *Biophys J* **107,** 2797-2814.

Deisseroth, K., Bito, H. and Tsien, R. W. (1996) Signaling from synapse to nucleus: postsynaptic CREB phosphorylation during multiple forms of hippocampal synaptic plasticity. *Neuron* **16,** 89-101.

Dixon, R. E., Moreno, C. M., Yuan, C., Opitz-Araya, X., Binder, M. D., Navedo, M. F. and Santana, L. F. (2015) Graded Ca^{2+}/calmodulin-dependent coupling of voltage-gated CaV1.2 channels. *Elife* **4**.

Dixon, R. E., Yuan, C., Cheng, E. P., Navedo, M. F. and Santana, L. F. (2012) Ca2+ signaling amplification by oligomerization of L-type Cav1.2 channels. *Proc Natl Acad Sci U S A* **109,** 1749-1754.

Dolphin, A. C. (2003) Beta subunits of voltage-gated calcium channels. *J Bioenerg Biomembr* **35,** 599-620.

Fallon, J. L., Baker, M. R., Xiong, L., Loy, R. E., Yang, G., Dirksen, R. T., Hamilton, S. L. and Quiocho, F. A. (2009) Crystal structure of dimeric cardiac L-type calcium channel regulatory domains bridged by Ca2+* calmodulins. *Proc Natl Acad Sci U S A* **106,** 5135-5140.

Folci, A., Steinberger, A., Lee, B. et al. (2018) Molecular mimicking of C-terminal phosphorylation tunes the surface dynamics of $Ca_V1.2$ calcium channels in hippocampal neurons. *J Biol Chem* **293,** 1040-1053.

Gao, T., Chien, A. J. and Hosey, M. M. (1999) Complexes of the alpha1C and beta subunits generate the necessary signal for membrane targeting of class C L-type calcium channels. *J Biol Chem* **274,** 2137-2144.

Grueter, C. E., Abiria, S. A., Wu, Y., Anderson, M. E. and Colbran, R. J. (2008) Differential regulated interactions of calcium/calmodulin-dependent protein kinase II with isoforms of voltage-gated calcium channel beta subunits. *Biochemistry* **47,** 1760-1767.

Hetzenauer, A., Sinnegger-Brauns, M. J., Striessnig, J. and Singewald, N. (2006) Brain activation pattern induced by stimulation of L-type Ca2+-channels: contribution of Ca(V)1.3 and Ca(V)1.2 isoforms. *Neuroscience* **139,** 1005-1015.

Hudmon, A., Schulman, H., Kim, J., Maltez, J. M., Tsien, R. W. and Pitt, G. S. (2005) CaMKII tethers to L-type Ca2+ channels, establishing a local and dedicated integrator of Ca2+ signals for facilitation. *J Cell Biol* **171,** 537-547.

Jarvis, S. E. and Zamponi, G. W. (2007) Trafficking and regulation of neuronal voltage-gated calcium channels. *Curr Opin Cell Biol* **19,** 474-482.

Jenkins, M. A., Christel, C. J., Jiao, Y., Abiria, S., Kim, K. Y., Usachev, Y. M., Obermair, G. J., Colbran, R. J. and Lee, A. (2010) Ca2+-dependent facilitation of Cav1.3 Ca2+ channels by densin and Ca2+/calmodulin-dependent protein kinase II. *J Neurosci* **30,** 5125-5135.

Jiao, Y., Jalan-Sakrikar, N., Robison, A. J., Baucum, A. J., Bass, M. A. and Colbran, R. J. (2011) Characterization of a central Ca2+/calmodulin-dependent protein kinase IIalpha/beta binding domain in densin that selectively modulates glutamate receptor subunit phosphorylation. *J Biol Chem* **286,** 24806-24818.

Koschak, A., Reimer, D., Huber, I., Grabner, M., Glossmann, H., Engel, J. and Striessnig, J. (2001) alpha 1D (Cav1.3) subunits can form l-type Ca2+ channels activating at negative voltages. *J Biol Chem* **276,** 22100-22106.

Koval, O. M., Guan, X., Wu, Y. et al. (2010) CaV1.2 beta-subunit coordinates CaMKII-triggered cardiomyocyte death and afterdepolarizations. *Proc Natl Acad Sci U S A* **107,** 4996-5000.

Li, Q., Lau, A., Morris, T. J., Guo, L., Fordyce, C. B. and Stanley, E. F. (2004) A syntaxin 1, Galpha(o), and N-type calcium channel complex at a presynaptic nerve terminal: analysis by quantitative immunocolocalization. *J Neurosci* **24,** 4070-4081.

Ma, H., Cohen, S., Li, B. and Tsien, R. W. (2012) Exploring the dominant role of Cav1 channels in signalling to the nucleus. *Biosci Rep* **33,** 97-101.

Ma, H., Groth, R. D., Cohen, S. M., Emery, J. F., Li, B., Hoedt, E., Zhang, G., Neubert, T. A. and Tsien, R. W. (2014) γCaMKII shuttles Ca^{2+}/CaM to the nucleus to trigger CREB phosphorylation and gene expression. *Cell* **159,** 281-294.

Ma, H., Khaled, H. G., Wang, X., Mandelberg, N. J., Cohen, S. M., He, X. and Tsien, R. W. (2023) Excitation-transcription coupling, neuronal gene expression and synaptic plasticity. *Nat Rev Neurosci* **24,** 672-692.

Marcantoni, A., Vandael, D. H., Mahapatra, S., Carabelli, V., Sinnegger-Brauns, M. J., Striessnig, J. and Carbone, E. (2010) Loss of Cav1.3 channels reveals the critical role of L-type and BK channel coupling in pacemaking mouse adrenal chromaffin cells. *J Neurosci* **30,** 491-504.

Moreno, C. M., Dixon, R. E., Tajada, S., Yuan, C., Opitz-Araya, X., Binder, M. D. and Santana, L. F. (2016) Ca(2+) entry into neurons is facilitated by cooperative gating of clustered CaV1.3 channels. *Elife* **5**.

Nakamura, Y., Reva, M. and DiGregorio, D. A. (2018) Variations in Ca^{2+} influx can alter chelator-based estimates of Ca^{2+} channle-synaptic vesicle coupling distance. *J Neurosci* **38,** 3971-3987.

Perfitt, T. L., Wang, X., Dickerson, M. T., Stephenson, J. R., Nakagawa, T., Jacobson, D. A. and Colbran, R. J. (2020) Neuronal L-Type Calcium Channel Signaling to the Nucleus Requires a Novel CaMKIIα-Shank3 Interaction. *J Neurosci* **40,** 2000-2014.

Pfeiffer, P., Egorov, A. V., Lorenz, F., Schleimer, J. H., Draguhn, A. and Schreiber, S. (2020) Clusters of cooperative ion channels enable a membrane-potential-based mechanism for short-term memory. *Elife* **9**.

Plante, A. E., Whitt, J. P. and Meredith, A. L. (2021) BK channel activation by L-type Ca^{2+} channels $Ca_V1.2$ and $Ca_V1.3$ during the subthreshold phase of an action potential. *J Neurophysiol* **126,** 427-439.

Richards, M. W., Butcher, A. J. and Dolphin, A. C. (2004) Ca2+ channel beta-subunits: structural insights AID our understanding. *Trends Pharmacol Sci* **25,** 626-632.

Robison, A. J., Bartlett, R. K., Bass, M. A. and Colbran, R. J. (2005) Differential modulation of Ca2+/calmodulin-dependent protein kinase II activity by regulated interactions with N-methyl-D-aspartate receptor NR2B subunits and alpha-actinin. *J Biol Chem* **280,** 39316-39323.

Shanks, N. F., Maruo, T., Farina, A. N., Ellisman, M. H. and Nakagawa, T. (2010) Contribution of the global subunit structure and stargazin on the maturation of AMPA receptors. *J Neurosci* **30,** 2728-2740.

Sheng, M. and Kim, E. (2000) The Shank family of scaffold proteins. *J Cell Sci* **113 (Pt 11),** 1851-1856.

Simms, B. A., Souza, I. A., Rehak, R. and Zamponi, G. W. (2015) The Cav1.2 N terminus contains a CaM kinase site that modulates channel trafficking and function. *Pflugers Arch* **467,** 677-686.

Stanika, R., Campiglio, M., Pinggera, A., Lee, A., Striessnig, J., Flucher, B. E. and Obermair, G. J. (2016) Splice variants of the $Ca_V1.3$ L-type calcium channel regulate dendritic spine morphology. *Sci Rep* **6,** 34528.

Strack, S., Robison, A. J., Bass, M. A. and Colbran, R. J. (2000) Association of calcium/calmodulin-dependent kinase II with developmentally regulated splice variants of the postsynaptic density protein densin-180. *J Biol Chem* **275,** 25061-25064.

Striessnig, J., Pinggera, A., Kaur, G., Bock, G. and Tuluc, P. (2014) L-type Ca^{2+} channels in heart and brain. *Wiley Interdiscip Rev Membr Transp Signal* **3,** 15-38.

Tadross, M. R., Tsien, R. W. and Yue, D. T. (2013) Ca2+ channel nanodomains boost local Ca2+ amplitude. *Proc Natl Acad Sci U S A* **110,** 15794-15799.

Vandael, D. H., Marcantoni, A., Mahapatra, S., Caro, A., Ruth, P., Zuccotti, A., Knipper, M. and Carbone, E. (2010) Ca(v)1.3 and BK channels for timing and regulating cell firing. *Mol Neurobiol* **42,** 185-198.

Vierra, N. C., Kirmiz, M., van der List, D., Santana, L. F. and Trimmer, J. S. (2019) Kv2.1 mediates spatial and functional coupling of L-type calcium channels and ryanodine receptors in mammalian neurons. *Elife* **8**.

Vierra, N. C., O'Dwyer, S. C., Matsumoto, C., Santana, L. F. and Trimmer, J. S. (2021) Regulation of neuronal excitation-transcription coupling by Kv2.1-induced clustering of somatic L-type Ca. *Proc Natl Acad Sci U S A* **118**.

Vivas, O., Moreno, C. M., Santana, L. F. and Hille, B. (2017) Proximal clustering between BK and Ca. *Elife* **6**.

Voigt, A., Freund, R., Heck, J., Missler, M., Obermair, G. J., Thomas, U. and Heine, M. (2016) Dynamic association of calcium channel subunits at the cellular membrane. *Neurophotonics* **3,** 041809.

Walikonis, R. S., Oguni, A., Khorosheva, E. M., Jeng, C. J., Asuncion, F. J. and Kennedy, M. B. (2001) Densin-180 forms a ternary complex with the (alpha)-subunit of Ca2+/calmodulin-dependent protein kinase II and (alpha)-actinin. *J Neurosci* **21,** 423-433.

Wang, X., Marks, C. R., Perfitt, T. L., Nakagawa, T., Lee, A., Jacobson, D. A. and Colbran, R. J. (2017) A novel mechanism for Ca2+/ calmodulin-dependent protein kinase II targeting

to L-type Ca2+ channels that initiates long-range signaling to the nucleus. *J Biol Chem* **292,** 17324-17336.

Weiss, N. and Zamponi, G. W. (2017) Trafficking of neuronal calcium channels. *Neuronal Signal* **1,** NS20160003.

Wheeler, D. G., Barrett, C. F., Groth, R. D., Safa, P. and Tsien, R. W. (2008) CaMKII locally encodes L-type channel activity to signal to nuclear CREB in excitation-transcription coupling. *J Cell Biol* **183,** 849-863.

Wheeler, D. G., Groth, R. D., Ma, H., Barrett, C. F., Owen, S. F., Safa, P. and Tsien, R. W. (2012) Ca(V)1 and Ca(V)2 channels engage distinct modes of Ca(2+) signaling to control CREB-dependent gene expression. *Cell* **149,** 1112-1124.

Wild, A. R., Sinnen, B. L., Dittmer, P. J., Kennedy, M. J., Sather, W. A. and Dell'Acqua, M. L. (2019) Synapse-to-Nucleus Communication through NFAT Is Mediated by L-type Ca2+ channel Ca2+ spike propagation to the soma. *Cell Rep* **26,** 3537-3550.e3534.

Wu, X. and Hammer, J. A. (2021) ZEISS Airyscan: Optimizing Usage for Fast, Gentle, Super-Resolution Imaging. *Methods Mol Biol* **2304,** 111-130.

Xu, W. and Lipscombe, D. (2001) Neuronal Ca(V)1.3alpha(1) L-type channels activate at relatively hyperpolarized membrane potentials and are incompletely inhibited by dihydropyridines. *J Neurosci* **21,** 5944-5951.

Yang, Q., Perfitt, T. L., Quay, J., Hu, L., Lawson-Qureshi, D. and Colbran, R. J. (2023) Clustering of $Ca_V1.3$ L-type calcium channels by Shank3. *J Neurochem* **167,** 16-37.

Zhang, H., Fu, Y., Altier, C., Platzer, J., Surmeier, D. J. and Bezprozvanny, I. (2006) Ca1.2 and CaV1.3 neuronal L-type calcium channels: differential targeting and signaling to pCREB. *Eur J Neurosci* **23,** 2297-2310.

Zhang, H., Maximov, A., Fu, Y., Xu, F., Tang, T. S., Tkatch, T., Surmeier, D. J. and Bezprozvanny, I. (2005) Association of CaV1.3 L-type calcium channels with Shank. *J Neurosci* **25,** 1037-1049.

Figures and legends

Figure 1. Activity-dependent regulation of dendritic $Ca_V1.3$ clustering in hippocampal neurons.

A) Schematic of neuronal transfection and experimental protocols. Rat primary hippocampal neurons were co-transfected with N-terminal intracellular HA-tagged $Ca_V1.3$ α1 subunit (iHA-$Ca_V1.3$) and FLAG-β2a at 14 days in vitro (DIV 14). At DIV 21, neurons were pre-incubated in 5K Tyrode's solution for 2 h and then stimulated for 90 s with either 5K or 40K Tyrode's solution. Neurons were immediately fixed, permeabilized and stained as described below. Detailed methods are provided in the Methods section.

B) Representative images of pCREB and DAPI staining in the soma. Scale bar, 10 µm.

C) Representative images of iHA-$Ca_V1.3$ staining in whole neurons (above) and dendrites (bottom) after 5K or 40K treatment. Scale bar, 20 µm for whole cells and 10 µm for enlarged dendrites.

D) Quantification of relative iHA-$Ca_V1.3$ cluster density and cluster intensity, respectively, in dendrites of n = 22 (5K) or 19 (40K) neurons from three independent cultures. Statistical analysis performed using an unpaired t-test.

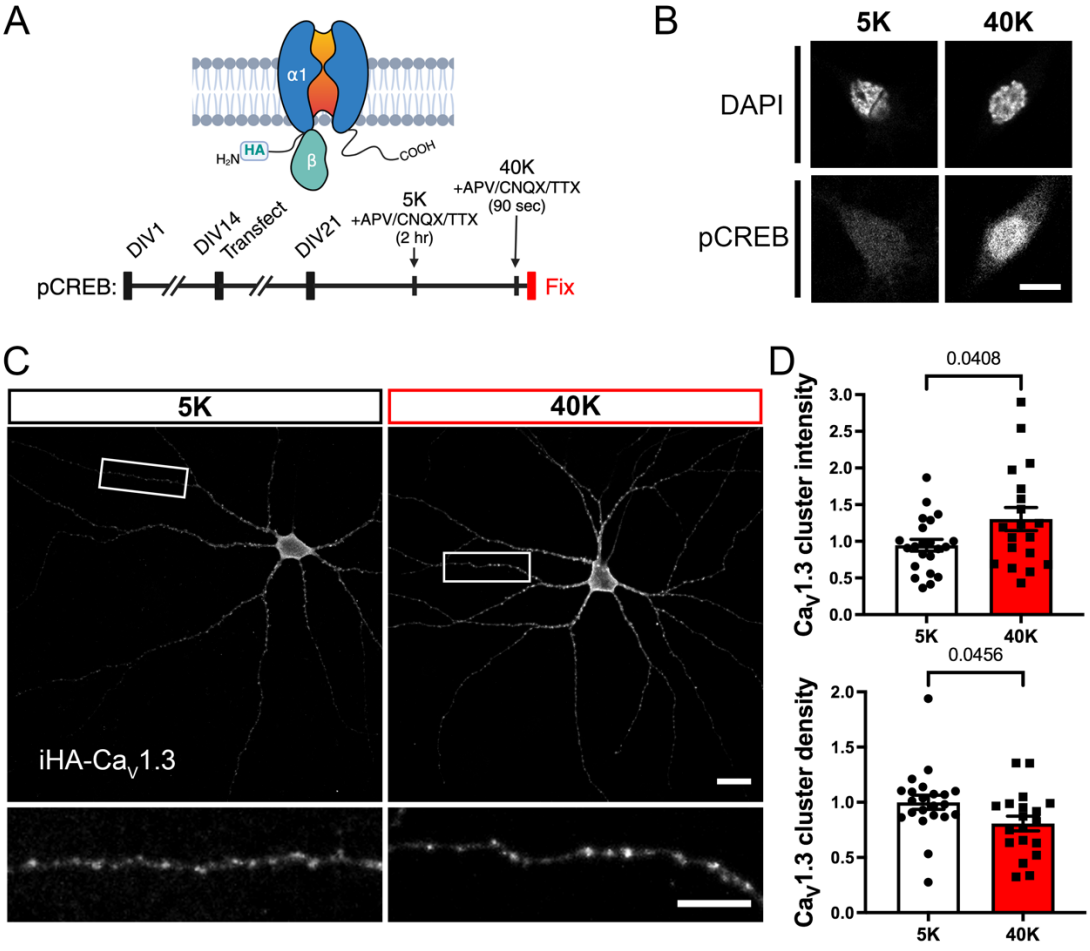

Figure 2. CaMKIIα-dependent assembly of $Ca_V1.3$ complexes after adding Ca^{2+}/CaM to HEK293T cell lysate.

A) Representative iHA, mCherry, CaMKII, and FLAG immunoblots in the input and anti-HA immunoprecipitations (IPs) from soluble fractions of HEK293T cells co-expressing iHA-$Ca_V1.3$, mCherry-$Ca_V1.3$, α2δ, FLAG-β3 or -β2a subunits, with or without CaMKIIα. Duplicate aliquots of the same lysates were immunoprecipitated with no further additions (EDTA) or following addition of Ca^{2+}/calmodulin (Ca^{2+}/CaM). Immunoblots were from the same replicate and images for each protein were collected from the same gel/blot using identical detection sensitivity.

B) Quantification of iHA-$Ca_V1.3$ and mCherry-$Ca_V1.3$ signals in HA-immune complexes from four independent transfection replicates. For each replicate, iHA-$Ca_V1.3$ signals in the IP lanes were normalized to the corresponding input (iHA-$Ca_V1.3$/input); mCherry-$Ca_V1.3$ signals were normalized to iHA-$Ca_V1.3$ in the corresponding lane (mCh/iHA-$Ca_V1.3$). Ratios within each replicate were then normalized to the "Ca^{2+}/calmodulin/β2a + CaMKII" condition to allow pooling of the data from all replicates. Statistical analysis: two-way ANOVA with Šídák's post hoc test.

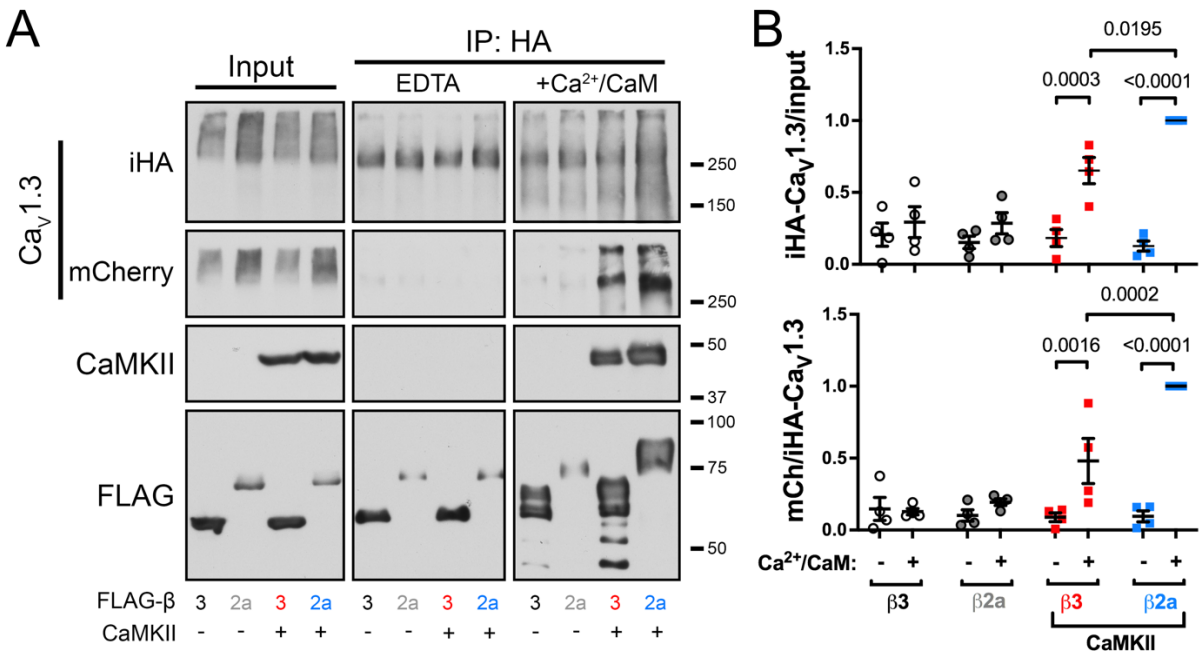

Figure 3. CaMKII-dependent assembly of $Ca_V1.3$/β2a complexes requires the addition of both Ca^{2+} and calmodulin.

A) Representative iHA, mCherry, FLAG-β2a, and CaMKII immunoblots in the input and anti-HA IPs from soluble fractions of HEK293T cells co-expressing iHA-$Ca_V1.3$, mCherry-$Ca_V1.3$, α2δ, and FLAG-β2a subunits, with or without CaMKII. Aliquots of the same lysates were supplemented with the addition of nothing, Ca^{2+} alone, calmodulin alone, or both Ca^{2+} and calmodulin.

B) Quantification of iHA-$Ca_V1.3$ and mCherry-$Ca_V1.3$ signals in HA-immune complexes from three independent transfection replicates. Immunoblot signals were normalized as described in the legend to figure 2, relative to the Ca^{2+}/calmodulin + CaMKII condition within each replicate. Statistical analysis: two-way ANOVA with Šídák's post hoc test (for comparisons without and with CaMKII co-expression) or by Tukey's post hoc test (for comparisons between four conditions).

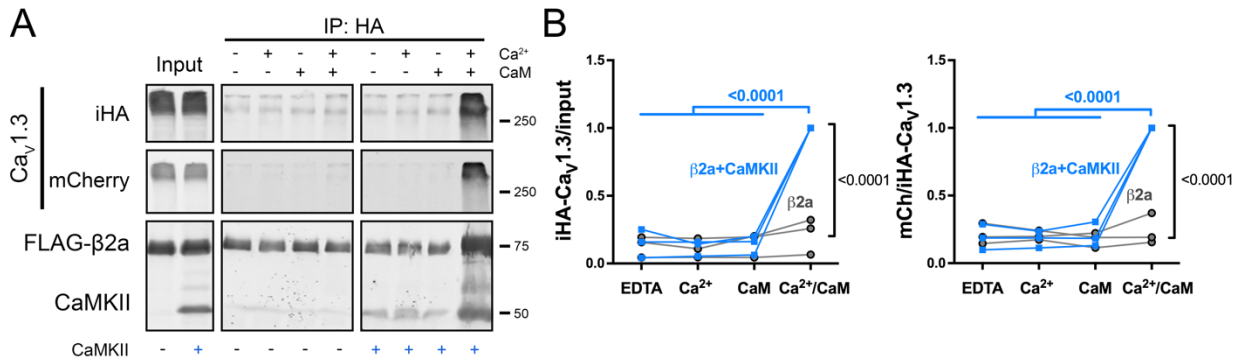

Figure 4. CaMKII- and Ca^{2+}/calmodulin-dependent assembly of $Ca_V1.3$/β2a complexes is unaffected by Shank3.

A) Representative iHA, mCherry, FLAG, GFP, and CaMKII immunoblots in the input and anti-HA IPs from soluble fractions of HEK293T cells co-expressing iHA- and mCherry-$Ca_V1.3$, α2δ, and FLAG-β2a subunits, along with GFP-Shank3/pcDNA or GFP/CaMKII or GFP-Shank3/CaMKII. Half of each lysate was supplemented with, Ca^{2+}/calmodulin prior to immunoprecipitation.

B) Quantification of iHA- and mCherry-$Ca_V1.3$, CaMKII, and GFP-Shank3 signals in HA-immune complexes from four independent transfection replicates. Immunoblot signals were normalized as described in the legend to figure 2, relative to the "Ca^{2+}/calmodulin + GFP-Shank3 + CaMKII" condition within each replicate. All data were analyzed using a two-way ANOVA followed by Šídák's post hoc test (for comparisons without and with Ca^{2+}/calmodulin condition) or by Tukey's post hoc test (for comparisons of iHA and mCh signals between different transfection conditions).

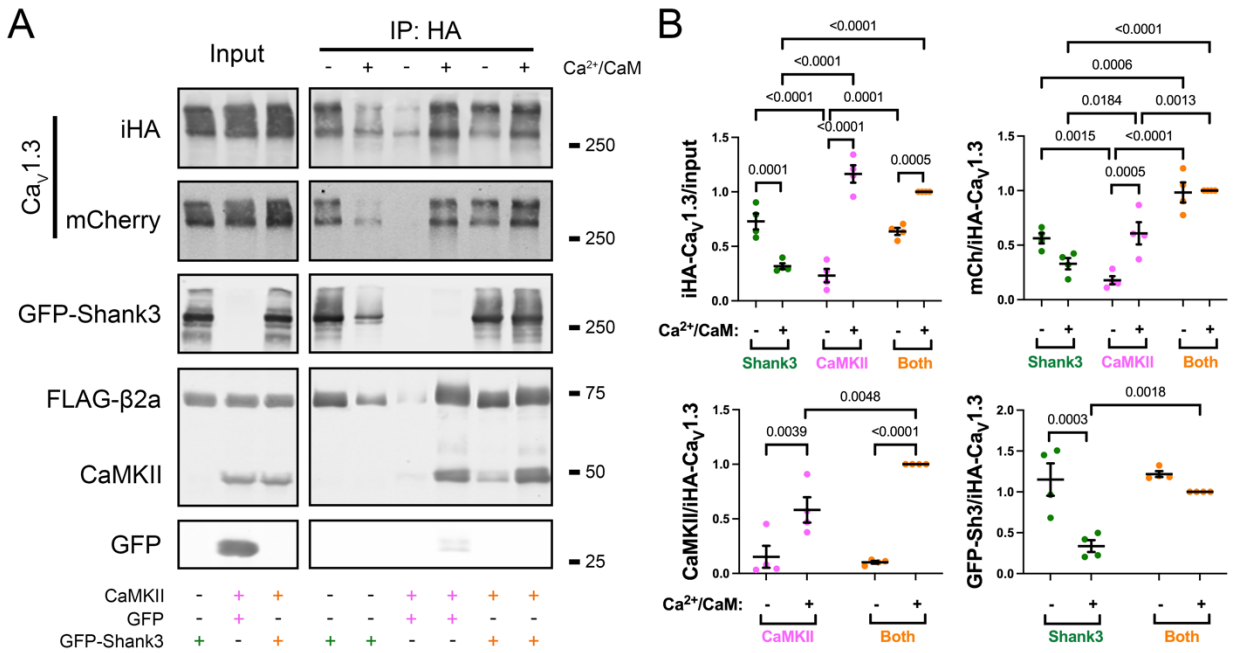

Figure 5. Activity- and CaMKIIα-dependent clustering of $Ca_V1.3$/β2a LTCCs in HEK 293 cells.
A) Representative iHA-$Ca_V1.3$, CaMKIIα and merged TIRF microscope images of fixed HEK293 cells co-expressing iHA-$Ca_V1.3$, α2δ, and FLAG-β2a subunits, and either empty pCDNA vector or CaMKIIα. Cells were fixed after 5-10 minutes incubation with either no Ca^{2+} or Ca^{2+} buffer with vehicle DMSO or BayK 8644 (BayK, 10 µM), as indicated (scale bar, 5 µm).
B-C) Quantification of iHA-$Ca_V1.3$ puncta intensity (panel B) and density (panel C) from 8-13 cells per condition from 4 independent transfection (pCDNA: n = 43 for DMSO, 43 for BayK, 40 for Ca^{2+}+DMSO, 45 for Ca^{2+}+BayK; CaMKII: n = 50 for DMSO, 42 for BayK, 45 for Ca^{2+}+DMSO, 47 for Ca^{2+}+BayK). Data within each replicate were normalized to the mean of values in the absence of Ca^{2+} and BayK 8644. Statistical analyses: two-way ANOVA followed by Šídák's (for comparisons between pCDNA and CaMKII) or Tukey's (for comparisons between different conditions) post hoc tests.

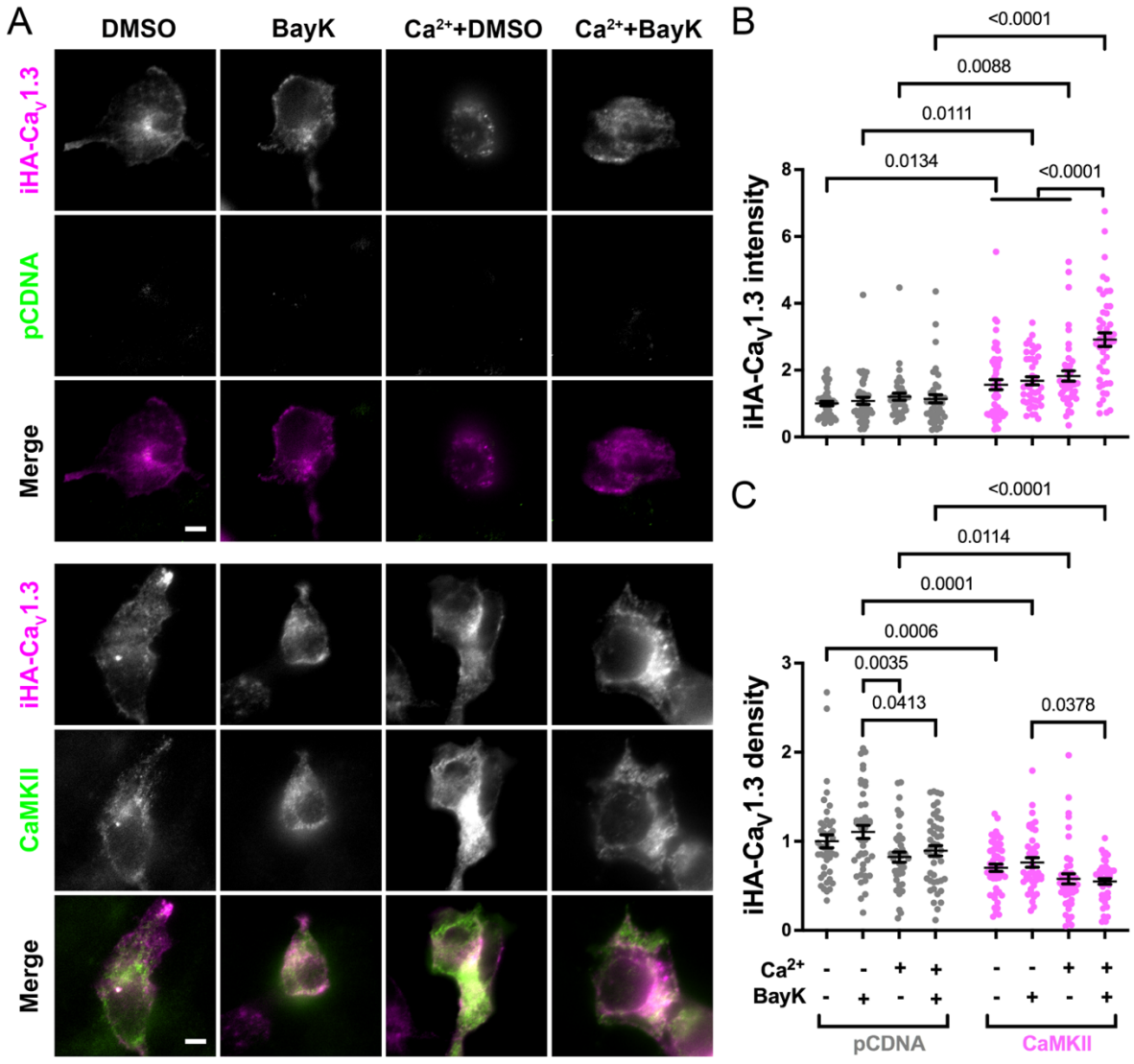

Figure 6. $Ca_V1.3/\beta2a$ LTCC clustering: influence of CaMKII-α1 subunit interaction.
A) Representative TIRF images of iHA-$Ca_V1.3$ and CaMKII in fixed HEK293 cells co-expressing iHA-$Ca_V1.3$, α2δ, and FLAG-β2a subunits, with wildtype CaMKII (WT) or CaMKII V102E mutant (V102E). Cells were incubated for approximately 5 min with zero Ca^{2+}(0 Ca^{2+}) or 2.5 mM Ca^{2+} and 10 µM BayK 8644 (Ca^{2+}+BayK) prior to fixation. Scale bar, 5 µm.
B) Quantification of iHA-$Ca_V1.3$ puncta intensity and density, as well as colocalization between iHA-$Ca_V1.3$ and CaMKII, respectively from three independent transfections. Data derived from n = 30 (0 Ca^{2+}) and 32 (Ca^{2+}+BayK) cells expressing WT CaMKII, and n = 26 (0 Ca^{2+}) and 30 (Ca^{2+}+BayK) cells expressing V102E CaMKII. The iHA puncta staining intensity and density values were normalized to the mean WT value in the absence of Ca^{2+} and BayK 8644 within each replicate. Statistical analysis: two-way ANOVA with Šídák's post hoc test.

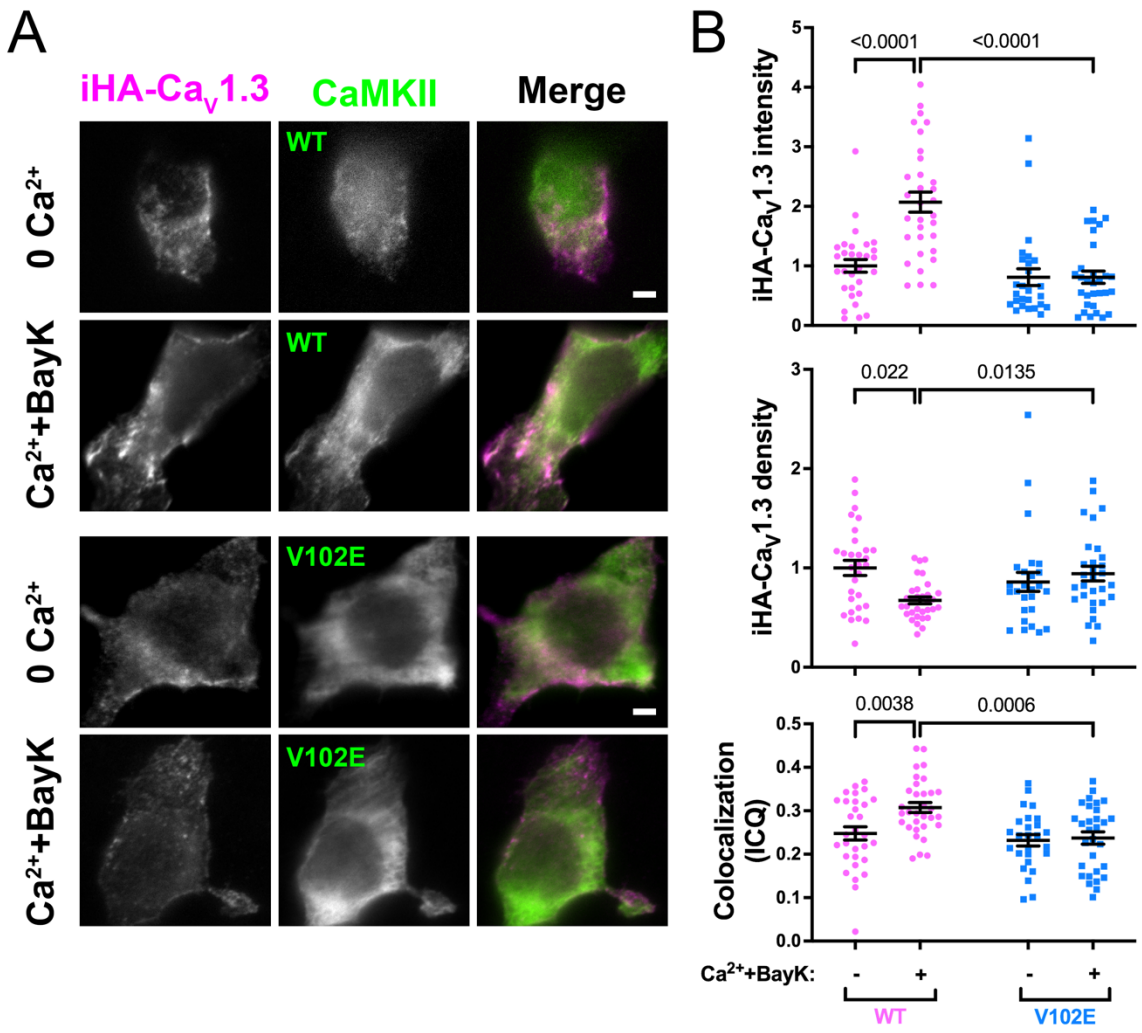

Figure 7. CaMKII is required for depolarization-induced CREB Ser133 phosphorylation in neurons over-expressing sHA-$Ca_V1.3$.

Primary rat hippocampal neurons (DIV 14) expressing $Ca_V1.3$ with an extracellular HA tag (sHA-$Ca_V1.3$) and FLAG-β3 or -β2a with either GFP-nonsense shRNA (nssh) or GFP-CaMKIIα shRNA/CaMKIIβ-shRNA (CaMKII-sh) were incubated for 90 s with 40K/5K at DIV 21 and fixed (see Figure 1). Neurons were immunostained for the HA tag without permeabilization and then permeabilized for staining for DAPI and pCREB (see methods). Images were collected using confocal microscopy.

A) Representative images of pCREB, DAPI, sHA, and GFP in neurons without (NT) or with transfection (nssh or CaMKII-sh). Scale bar, 5 µm.

B) Quantification of pCREB signal after 5K or 40K treatment in neurons with or without nssh expression (NT: n = 129 for 5K and 141 for 40K; nssh: n = 41 for 5K and 40 for 40K).

C) Quantification of pCREB signal after 5K or 40K treatment in neurons with or without CaMKII-sh expression (NT: n = 113 for 5K and 204 for 40K; nssh: n = 41 for 5K and 50 for 40K).

Data were collected from four independent transfections and normalized to the mean for non-transfected neurons following the 40K incubation within each replicate. Statistical analyses: two-way ANOVA with Tukey's post hoc test.

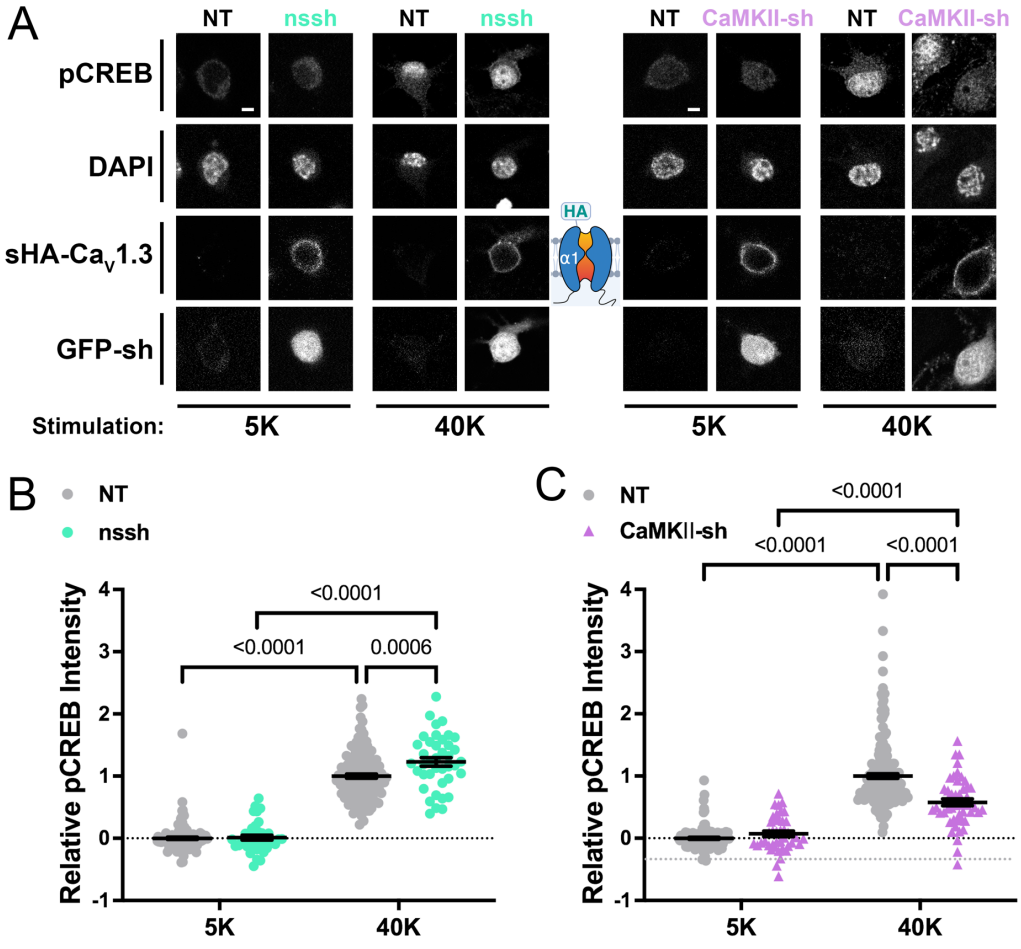

Figure 8. Depolarization-induced $Ca_V1.3$ clustering in hippocampal neurons is disrupted by CaMKII knockdown.

Primary rat hippocampal neurons expressing sHA-$Ca_V1.3$ and FLAG-β2a with either GFP-nssh or GFP-CaMKII-sh (DIV 21) were incubated for 90 s with 40K or 5K and then fixed (see Figure 1). Neurons were immunostained for HA prior to permeabilization and then permeabilized for endogenous CaMKII immunostaining (eCaMKII) (see methods). Images collected using Airyscan super-resolution confocal microscopy.

A) Representative images of sHA and CaMKII staining in soma and dendrites of neurons expressing GFP-nssh. Scale bar, 5 µm.

B-C) Quantification of sHA-$Ca_V1.3$ cluster intensity and density in soma (B) and dendrites (C)of n = 41 (5K) and 33 (40K) GFP-nssh expressing neurons.

D) Representative images of sHA and CaMKII staining in soma and dendrites of neurons expressing GFP-CaMKII-sh. Scale bar, 5 µm.

E-F) Quantification of sHA-$Ca_V1.3$ cluster intensity and density in soma (n = 34 (5K) and 28 (40K)) (E) and Dendrites (n = 33 (5K) and 27 (40K) (F) of neurons expressing GFP-CaMKII-sh. Note that we detected only two secondary dendrites in one neuron in each condition so only the soma was analyzed.

Data were quantified from 5 independent cultures/transfections and normalized to the mean for non-transfected neurons following the 5K incubation within each replicate. All statistical comparisons used unpaired t-tests.

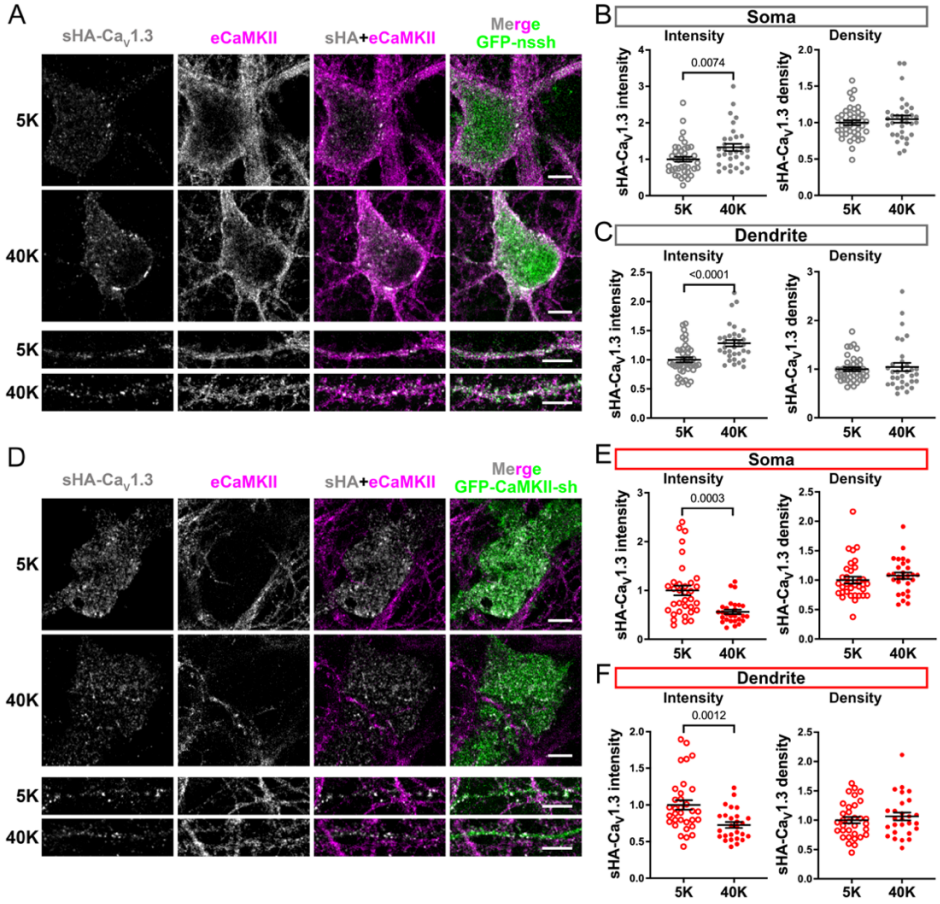

Figure 9. Hippocampal neuron depolarization also increases $Ca_V1.2$ LTCCs clustering by a CaMKII-dependent mechanism.

Primary rat hippocampal neurons expressing sHA-$Ca_V1.2$ and FLAG-β2a with either GFP-nssh or GFP-CaMKII-sh (DIV 21) were incubated for 90 s with 40K/5K and fixed (see Figure 1). Neurons were immunostained for HA prior to permeabilization and then permeabilized for endogenous CaMKII immunostaining (eCaMKII) (see methods). Images collected using Airyscan super-resolution confocal microscopy.

A) Representative images of sHA and CaMKII staining in soma and dendrites of neurons expressing GFP-nssh. Scale bar, 5 µm.

B-C) Quantification of sHA-$Ca_V1.2$ cluster intensity and density in soma (Panel B) and dendrites (Panel C) of n = 24 (5K) and 27 (40K) neurons expressing GFP-nssh.

D) Representative images of sHA and CaMKII staining in soma and dendrites of neurons expressing GFP-CaMKII-sh. Scale bar, 5 µm.

E-F) Quantification of sHA-$Ca_V1.2$ cluster intensity and density in soma (panel E) and dendrites (panel F) of n = 27 (5K) and 24 (40K) neurons expressing GFP-CaMKII-sh.

Data were quantified from 3 independent cultures/transfections and normalized to the mean for non-transfected neurons following the 5K incubation within each replicate. All statistical comparisons used unpaired t-tests.

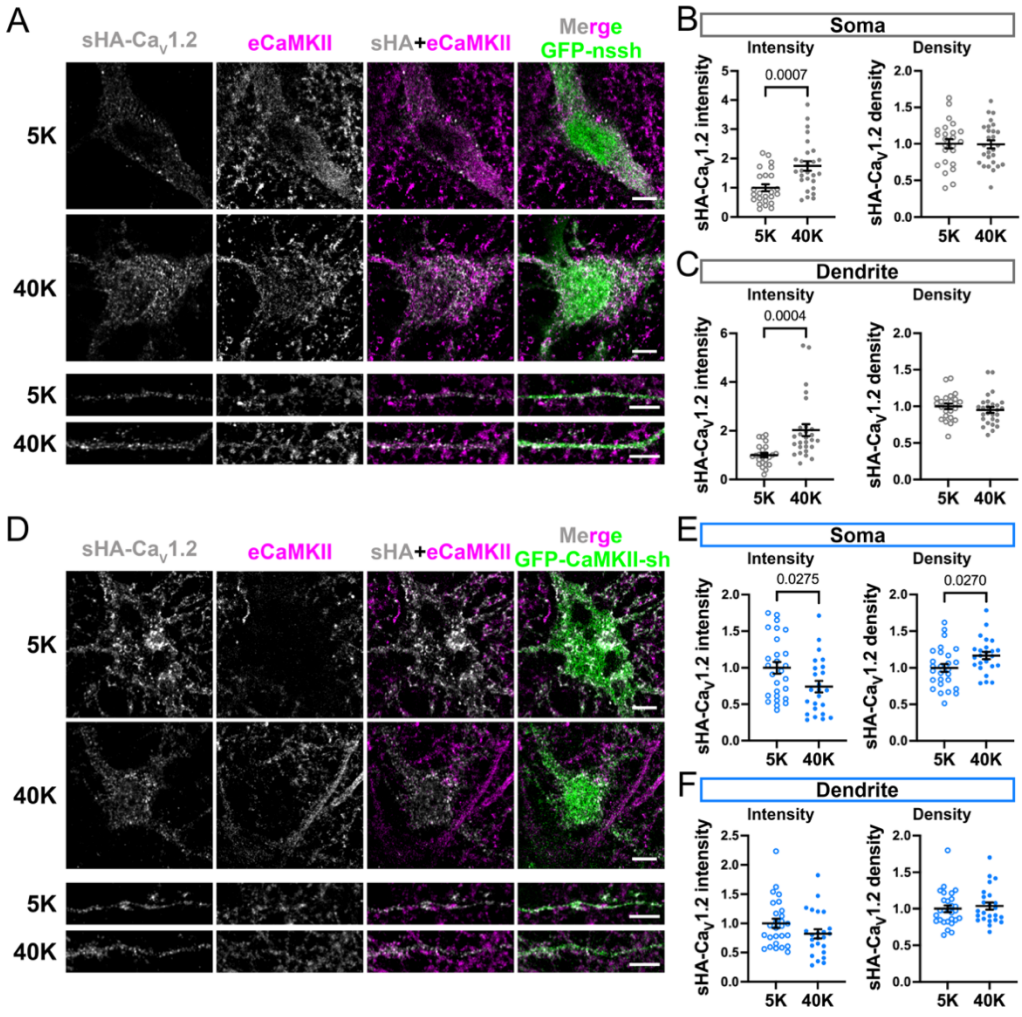

Figure 10. CaMKIIα- and Ca^{2+}/calmodulin-dependent assembly of $Ca_V1.2$/$Ca_V1.3$ complexes in HEK293T cell lysates.

A) Representative immunoblots of iHA, GFP, FLAG, and CaMKIIα in the input and anti-HA IPs from soluble fractions of HEK293T cells co-expressing iHA-$Ca_V1.3$, GFP-$Ca_V1.2$, α2δ, and FLAG-β2a subunits, with or without CaMKIIα, and without or with Ca^{2+}/calmodulin addition.

B) Quantification of iHA-$Ca_V1.3$, GFP-$Ca_V1.2$, FLAG-β2a, and CaMKIIα signals in HA-immune complexes from three independent transfection replicates. Immunoblot signals were normalized as described in the legend to figure 2, relative to the Ca^{2+}/calmodulin condition with CaMKII co-expression.

C) Immunoblots illustrating representative signals of iHA, GFP, FLAG, and CaMKIIα in the input and anti-HA IPs from soluble fractions of HEK293T cells co-expressing iHA-$Ca_V1.3$, GFP-$Ca_V1.2$, α2δ, FLAG-β2a subunits, and CaMKIIα (WT or V102E mutant) without or with Ca^{2+}/calmodulin addition.

D) Quantification of iHA-$Ca_V1.3$ and GFP-$Ca_V1.2$ signals in HA-immune complexes from four independent transfection replicates. Immunoblot signals were normalized as described in the legend to figure 2, relative to the Ca^{2+}/calmodulin condition with CaMKII-WT co-expression.

All statistical analyses used a two-way ANOVA with Šídák's post hoc test.

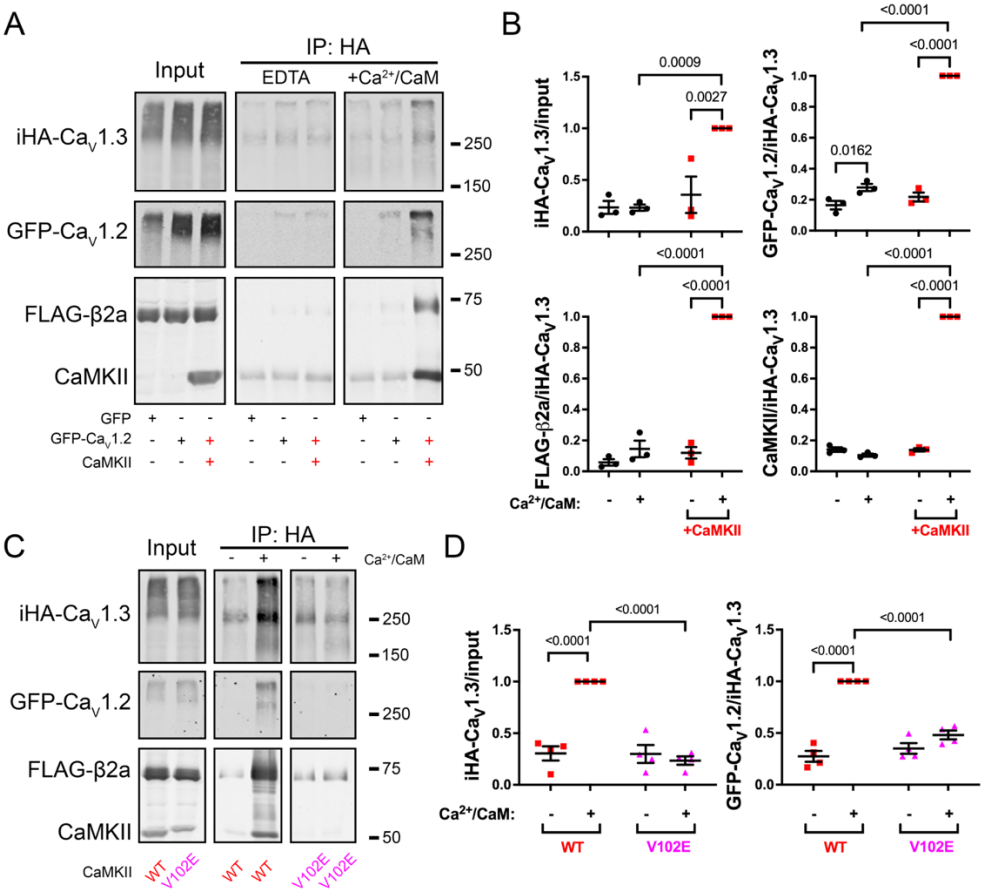

Figure 11. Depolarization-induced $Ca_V1.3$-$Ca_V1.2$ co-clustering is CaMKII-dependent in hippocampal neurons.

Primary rat hippocampal neurons expressing sHA-$Ca_V1.3$ and FLAG-β2a with either GFP-nssh or GFP-CaMKII-sh (DIV21) were incubated for 90 s with 40K/5K and fixed (see Figure 1). Neurons were immunostained for HA prior to permeabilization for endogenous $Ca_V1.2$ ($eCa_V1.2$) staining. Neurons were imaged using an Airyscan super-resolution confocal microscopy.
A and B) Representative images of sHA staining, $eCa_V1.2$ staining, and merged images in soma (A) and on dendrites (B) of neurons expressing GFP-nssh or CaMKII-sh. Scale bar, 5 µm.
C and D) ROIs were defined based on sHA staining in order to measure the ratio of normalized $eCa_V1.2$ intensity to normalized sHA intensity in somatic (C) and dendritic (D) Quantification of $eCa_V1.2$ staining within sHA-$Ca_V1.3$ ROIs (see methods) in neurons from four independent transfected cultures. n = 20 (5K) and 21 (40K) neurons expressing nssh; n = 20 (5K) and 22 (40K) neurons expressing CaMKII-sh. Data were normalized to the average $eCa_V1.2$/sHA-$Ca_V1.3$ ratio in nssh neurons with 5K treatment for each transfection. Statistical analysis: two-way ANOVA with Šídák's post hoc test.

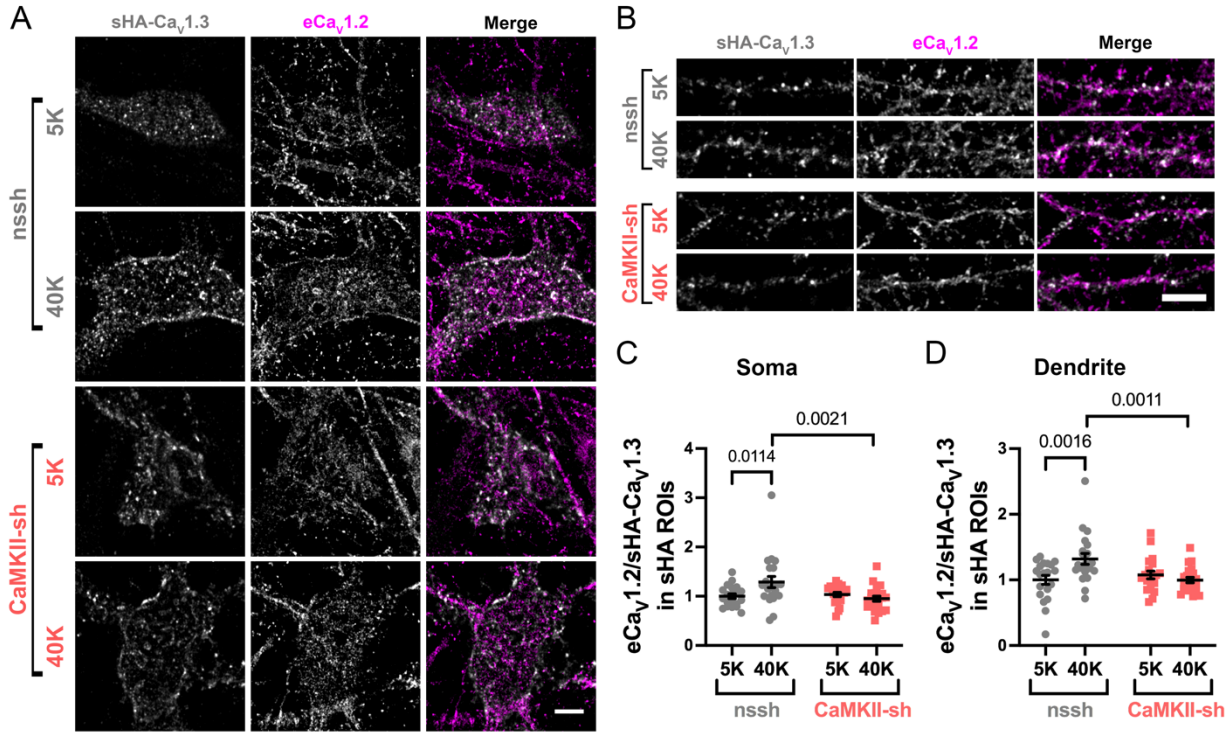

Figure 12. Proposed model for Ca^{2+}-induced CaMKII mediated co-clustering of $Ca_V1.3$ and $Ca_V1.2$ in nanodomains.

$Ca_V1.3$ and $Ca_V1.2$ LTCCs are organized in separate clusters in the plasma membrane of hippocampal neurons at hyperpolarized membrane potentials, but the clusters contain a relatively small number of $Ca_V1.3$ and $Ca_V1.2$ LTCCs. $Ca_V1.3$ is selectively activated by weaker membrane depolarization and the initial Ca^{2+} influx activates CaMKII, recruiting it to $Ca_V1.3$ to enlarge the clusters. This amplifies activation of CaMKII dodecameric holoenzyme to serve as a scaffolding protein that nucleates the assembly of multimeric $Ca_V1.2$-$Ca_V1.3$ co-clusters. The collective Ca^{2+} influx through clustered LTCCs creates a local Ca^{2+} nanodomain (yellow gradient) that initiates LTCC-dependent E-T coupling.